

# Variational analysis of the influence of grain shape anisotropy on shear viscosity in Nabarro-Herring-Coble creep

Francis Delannay<sup>a\*</sup> and Laurence Brassart<sup>b</sup>

<sup>a</sup> Université catholique de Louvain, Institute of Mechanics, Materials and Civil Engineering, iMMC/IMAP, Place Sainte Barbe 2, B-1348 Louvain-la-Neuve, Belgium, francis.delannay@uclouvain.be.

<sup>b</sup> University of Oxford, Department of Engineering Science, Parks Road, Oxford OX1 3PJ, UK, and Monash University, Department of Materials Science and Engineering, 22 Alliance Lane, Clayton, VIC 3800, Australia, laurence.brassart@eng.ox.ac.uk

## Abstract

The effect of strain-induced grain shape anisotropy on diffusional creep viscosity is analysed in two dimensions via a model representing grains by cylinders with elliptical cross section. Both cases of dominance of grain boundary diffusion and lattice diffusion are considered. Anisotropic creep viscosity is described by two coefficients calculated by considering different loading configurations with respect to the ellipse axes. Upper and lower bounds on these coefficients are obtained using kinematic and statical variational principles and assuming affine velocity, or uniform stress trial boundary fields, respectively. The analysis emphasises the dependence of the viscosity coefficients on aspect ratio and grain boundary viscosity. The difference between the bounds increases with grain elongation. A method is proposed for deriving estimates for the effective viscosity coefficients by coupling the two bounds. The strain hardening effect is analysed. Lattice diffusion contributes less to viscosity anisotropy than diffusion and sliding at grain boundaries.

**Keywords :** Diffusional creep, viscosity anisotropy, variational principles, grain boundary sliding

\* Corresponding author: [francis.delannay@uclouvain.be](mailto:francis.delannay@uclouvain.be). Tél +32479738784

Table 1 : list of symbols*Material properties and physical constants*

$k$	Boltzmann's constant (energy per atom and per Kelvin)
$D_b$	grain boundary diffusion coefficient (area per unit time)
$D_l$	lattice diffusion coefficient (area per unit time)
$\eta$	boundary viscosity coefficient at grain boundary (force * time per unit volume)
$\eta_b$	boundary viscosity coefficient defined in Eq. (56) (non-dimensional)
$\eta_l$	boundary viscosity coefficient defined in Eq. (63) (non-dimensional)
$\Omega$	volume per atom

*Scalars and scalar functions*

$a$	half major axis of ellipse
$b$	half minor axis of ellipse
$c$	geometrical parameter defined in Eq. (56) (non-dimensional)
$e$	geometrical parameter defined in Eq. (41) (non-dimensional)
$s$	curvilinear coordinate along ellipse boundary
$A(\phi)$	function of $\phi$ defined in Eq. (42) (non-dimensional)
$B(\phi)$	function of $\phi$ defined in Eq. (38) (non-dimensional)
$E$	total accumulated strain along principal tensile direction
$\dot{E}$	macroscopic strain rate along principal tensile direction
$F_b(\alpha)$	integration constant defined in Eq. (55) (non-dimensional)
$G$	isotropic shear viscosity (force * time per unit surface)
$R_G$	radius of circular cylinder with same cross sectional area as grain average
$S$	macroscopic stress along principal tensile direction
$V$	grain volume
$\alpha$	rotation of coordinate system axes with respect ellipse axes
$\beta$	orientation of normal vector $\mathbf{n}$ with respect to coordinate axis 2 (Fig. 2)
$\gamma$	parameter defined in Eq. (74) (non-dimensional)
$\delta$	thickness of grain boundary layer

$\phi$	azimuthal coordinate defined in Fig. 2
$\lambda(\alpha)$	function defined in Eqs. (62) (non-dimensional)
$\mu$	diffusion potential (energy per atom)
$\theta$	azimuthal angle defined with respect to coordinate axis 2 (Fig. 2)
$\dot{\theta}$	grain rotation velocity
$\rho$	radial coordinate defined in Fig. 2
$\Phi$	dissipation potential defined by Eq. (33) (energy per unit time per unit volume)
$\Psi$	dissipation potential defined by Eq. (30) (energy per unit time per unit volume)

*Vectors, tensors, and matrices*

<b>c</b>	viscous stiffness matrix (force * time per unit surface)
<b>n</b>	unit vector normal to ellipse
$j_b$	grain boundary diffusion flux (volume per unit length per unit time)
<b>s</b>	viscous compliance matrix (surface per unit force per unit time)
<b>t</b>	unit vector tangent to ellipse
$\dot{\mathbf{u}}$	local velocity vector
<b>x</b>	position vector
$\dot{\mathbf{E}}$	macroscopic strain rate tensor
<b>F</b>	force on the grain per unit grain thickness
<b>M</b>	moment on the grain per unit grain thickness
<b>R</b>	vector connecting grain centroid to grain boundary
$J_l$	lattice diffusion flux (volume per unit surface per unit time)
<b>S</b>	macroscopic stress tensor
<b>T</b>	traction vector on ellipse boundary
$\dot{\boldsymbol{\varepsilon}}$	local strain rate tensor
$\boldsymbol{\sigma}$	local stress tensor
$\Delta \dot{\mathbf{u}}$	velocity jump vector at ellipse boundary

## 1. Introduction

According to the Nabarro-Herring-Coble (NHC) deformation model, deformation of a polycrystal can arise without dislocation activity by means of the coupling of emission/absorption of vacancies at grain boundaries and sliding along grain boundaries (Nabarro, 1948) (Herring, 1950) (Coble, 1963) (Lifshitz, 1963). This model is commonly invoked for apprehending such phenomena as the creep rate and superplastic behaviour of a dense polycrystal under low stress, the sintering of a porous aggregate of grains, and the rheology of crystalline rocks in the Earth's mantle (Rudge, 2018; Takei and Holtzman, 2009; Wheeler, 2009). Since the pioneering papers of Nabarro, Herring, Coble, and Lifshitz, many authors have, via three-dimensional (3D) or two-dimensional (2D) models, contributed to improve the understanding of the link between the shear viscosity of the body – i.e. the steady-state deformation rate at constant volume – and the physical parameters governing the NHC deformation of a randomly isotropic polycrystal (Beere, 1977; Green, 1970; Kim et al., 2004; McMeeking and Kuhn, 1992; Mori et al., 1997; Mori et al., 1998a; Mori et al., 1998b; Onaka et al., 2001; Pan and Cocks, 1993; Raj and Ashby, 1971; Spingarn and Nix, 1978). The main parameters of the models are the average grain size,  $R_G$ , the diffusion coefficients in the lattice and at grain boundaries,  $D_l$  and  $D_b$ , and the boundary viscosity coefficient,  $\eta$ , which controls grain boundary sliding. Experimental validation of the models is however difficult owing in particular to the lack of experimental data on the value to be ascribed to  $\eta$ .

In comparison, fewer studies have considered the case of textured polycrystals in which grains are elongated in preferential directions. This situation typically arises during finite deformation. The original NHC model involves the hypothesis that grain deformation arises primarily from diffusion phenomena and that the role of grain boundary sliding is limited to

maintaining deformation compatibility between grains. The original NHC model thus implies that the deformation of individual grains is, on average, equal to the macroscopic deformation of the polycrystal. However several authors have shown that, during NHC deformation, maintenance of an equiaxed microstructure at large strain can be favoured by the occurrence of “grain neighbour switching” events (Ashby and Verrall, 1973; Lee, 1970). In addition, Cannon (Cannon, 1972) introduced the distinction between the NHC deformation mode and the “Rachinger sliding” mode (Rachinger, 1952) in which individual grains remain, on average, equiaxed owing to a deformation mode involving primarily rearrangements by translation of grains relative to one another. The role of diffusion is then limited to maintaining deformation compatibility between grains. We consider in this work only the original NHC deformation mode, i.e. we consider that finite deformation brings the polycrystal to become textured with all grains elongated in the same direction.

Several authors have attempted to capture the evolution of the NHC creep rate during straining by considering lattices of polyhedral (3D) or polygonal (2D) grains with elongated unit cells, usually assuming  $\eta = 0$  (Burton, 1994; Burton and Greenwood, 1985; Greenwood, 1992; Kim et al., 2004; Kim et al., 2003; Li et al., 2015; Wheeler, 2010). The problem is complex because the behaviour strongly depends on the orientation of the strain rate tensor with respect to the unit cell. For example, it was shown by Kim *et al* (Kim et al., 2004; Kim et al., 2003) that, for 2D hexagonal lattices, the uniaxial creep rate increases with increasing grain aspect ratio if two sides of the hexagonal unit cell are perpendicular to the tensile axis, whereas the reverse is observed if two sides are parallel to the tensile axis. The reason is that the effect of the decrease of the size of some of the grain facets may be larger than the effect of the overall increase of diffusion distances. Another example is the work of Wheeler who analysed the role

of grain rotation and its influence on viscosity anisotropy by considering lattices made of deformed hexagonal unit cells with variable aspect ratio (Wheeler, 2010). Wheeler showed that polycrystal viscosity is extremely anisotropic if grain boundary viscosity is null, and that, although anisotropy is less extreme, weak directions still exist when  $\eta > 0$ . The complexity is related to the fact that deformed hexagons are characterised by four parameters. In the present work, this complexity is alleviated by representing the grain by an ellipse, of which the characterizing parameter is the aspect ratio only.

In a recent paper (Brassart and Delannay, 2019), the present authors have revisited the shear viscosity of randomly isotropic polycrystals with equiaxed grains undergoing NHC deformation by applying two variational principles in a model considering, like Herring and Coble (Herring, 1950) (Coble, 1963), a spherical representation of the grain. The kinematic principle establishes that an upper bound for the shear viscosity is obtained if the stress potential is calculated for any admissible trial grain boundary velocity field and diffusion flux field compatible with prescribed macroscopic strain rate. The kinematic/upper bound derived using affine boundary velocity conditions was consistent with the solution reported by previous authors (Herring, 1950) (Coble, 1963) (Onaka et al., 2001). The statical principle establishes that a lower bound is obtained if the strain rate potential is calculated for any admissible trial grain boundary traction field and diffusion potential field compatible with prescribed macroscopic stress. This statical/lower bound was derived using uniform boundary traction conditions. The objective of the present paper is to apply the same variational method for analysing the link between grain shape anisotropy and viscosity anisotropy in a polycrystal with grains having initially equiaxed shapes with random orientation.

Modelling principles are presented in Section 2. The average grain is represented in 2D by a circular cylinder of which the cross-section becomes an ellipse. The increasing aspect ratio is a measure of the strain-induced shape anisotropy in the polycrystal. Viscosity anisotropy is characterised two viscosity coefficients to be properly chosen. For the kinematic bound, the trial grain boundary velocity field is defined by assuming affine displacement of grain centroids without grain translation and rotation. For the statical bound, the trial grain boundary traction field is defined by assuming a uniform stress field. In Section 3, kinematic and statical bounds for the two viscosity coefficients are calculated for both cases of grain boundary diffusion and lattice diffusion. For conciseness, only the major results are presented: details of mathematical developments are provided in the “Supplementary Material” document appended to the paper. Section 4 begins with an analysis of the results for equiaxed grains, supported by a comparison with previous models based on a circular grain shape or on a lattice of regular hexagons. A critical evaluation is then made of whether the two types of boundary conditions are realistic for a random polycrystal. The discussion finally focusses on the dependence of viscosity anisotropy on the dominant diffusion mechanism, on boundary viscosity, and on grain aspect ratio. Appendix 1 assesses whether the solutions ensuing from the chosen boundary conditions are exact or not. Appendix 2 shows that, for equiaxed grains, there exists no other exact solution than the kinematic and statical bounds.

## 2. Principles

We consider a fully dense, randomly isotropic, 2D polycrystal with all grains infinitely elongated in the transverse direction. As only three grain boundaries can meet along a grain boundary junction, the average grain coordination number in a 2D polycrystal is six (the average

coordination number can decrease in the presence of porosity because more than three grain boundaries can meet along a pore channel). In the presence of grain shape anisotropy, the average grain shape is thus an asymmetric hexagon. A statistical measure of grain shape anisotropy can be the orientation distribution of the distance between the centroids of two adjacent grains. We assume that the grains can be represented by an average elliptical cylinder with aspect ratio best fitting the polygonal grains. An elliptical representation of the grains should allow alleviating some of the complexities arising from a polygonal representation (Kim et al., 2004; Wheeler, 2010). We further assume that the orientation distribution of the distance between the centroids of two adjacent grains is elliptical and described by the same aspect ratio (Fig. 1). Note that this is not necessarily the case in real microstructure, as the elliptical distribution of grain centroid may differ from the average elliptical grain shape (Ponte-Castañeda and Willis, 1995).

The principal axes of the ellipse are denoted  $2a$  and  $2b$  with, by convention,  $a > b$ . The area of the ellipse is taken to be the average cross-sectional area of the grains:

$$\sqrt{ab} = R_G \quad (1)$$

where  $R_G$  is the radius of a circular cylinder with cross sectional area equal to the average grain cross section.

We will deal only with the steady-state stage of deformation and neglect the transient stage during which stress and velocity fields evolve after the onset of loading (the transient stage has been analysed by Mori, Onaka et al (Mori et al., 1998a; Onaka et al., 1998) based on a two-dimensional model with equiaxed grains). Steady-state macroscopic strain rate tensor and stress tensor will be written  $\dot{\mathbf{E}}$  and  $\mathbf{S}$ . If grain elongation results from the deformation of an initially random polycrystal with equiaxed grains, deformation brings about a texture, i.e. a



preferential orientation, which can be captured via the evolution of the aspect ratio  $a/b$  and of the orientation of the axes of the ellipse as a function of strain. If principal strain directions do not change during straining, the aspect ratio is related to the strain in the principal tensile direction,  $E$ , as

$$E = \ln \frac{a}{R_G} = \ln \sqrt{\frac{a}{b}}. \quad (2)$$

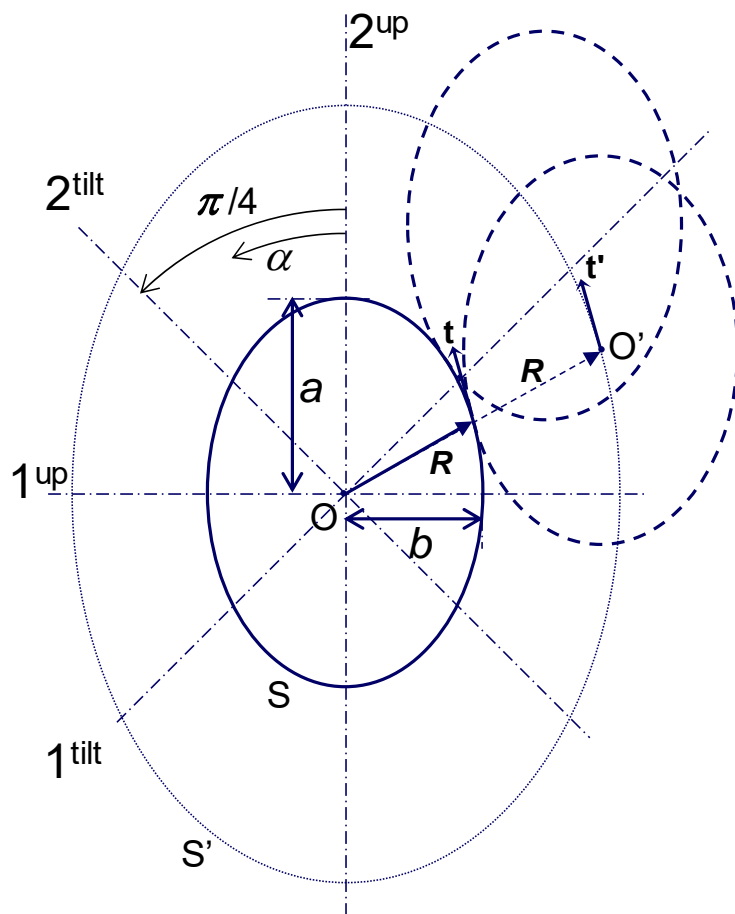


**Figure 1:** Statistical model representing grains as elliptical cylinders with principal axes oriented in the same direction. Angle  $\alpha$  represents a rotation of the coordinate system around axis 3.

### 2.1. Macroscopic viscosity anisotropy: two-dimensional analysis

As represented in Figure 1, we consider an orthogonal coordinate system with axes 1 and 2 in the plane. Deformation along axis 3 requires diffusional exchange of matter between grain boundaries and external surfaces. Infinite elongation in direction 3 thus means that deformation along axis 3 is negligible, i.e. deformation is fully plane strain. Angle  $\alpha$  defines the angle of (anticlockwise) rotation of axes 2 and 1 with respect to axes  $a$  and  $b$  of the ellipse, respectively. The coordinate system with  $\alpha = 0$  will be designated by superscript “up” for referring to the “upright” orientation of the ellipse, whereas the coordinate system with  $\alpha = \frac{\pi}{4}$  will be designated by superscript “tilt” for referring to the “tilted” orientation of the ellipse.

A linear relation is assumed between strain rate and stress. For the definition of the viscous compliance and stiffness matrices,  $\mathbf{s}$  and  $\mathbf{c}$ , we follow Voigt’s notation for the array representation of stress and strain rate tensors (Nye, 1957). If all grains have the same orientation, we expect the effective properties to be orthotropic with two mirror planes parallel to the ellipse axes and the third mirror plane parallel to the plane of the ellipse. It follows from the symmetry properties of strain rate and stress tensors that, if the coordinate axes are aligned with ellipse axes, i.e. if  $\alpha = 0$ , the two-dimensional viscous matrices of a compressible orthotropic material under plane strain,  $\mathbf{s}^{\text{up}}$  and  $\mathbf{c}^{\text{up}}$ , reduce to

$$\begin{pmatrix} \dot{E}_{11} \\ \dot{E}_{22} \\ 2\dot{E}_{12} \end{pmatrix} = \begin{pmatrix} s_{11}^{\text{up}} & s_{12}^{\text{up}} & 0 \\ s_{12}^{\text{up}} & s_{22}^{\text{up}} & 0 \\ 0 & 0 & s_{66}^{\text{up}} \end{pmatrix} \begin{pmatrix} S_{11} \\ S_{22} \\ S_{12} \end{pmatrix} \quad (3)$$

$$\text{and} \quad \begin{pmatrix} S_{11} \\ S_{22} \\ S_{12} \end{pmatrix} = \begin{pmatrix} c_{11}^{\text{up}} & c_{12}^{\text{up}} & 0 \\ c_{12}^{\text{up}} & c_{22}^{\text{up}} & 0 \\ 0 & 0 & c_{66}^{\text{up}} \end{pmatrix} \begin{pmatrix} \dot{E}_{11} \\ \dot{E}_{22} \\ 2\dot{E}_{12} \end{pmatrix} \quad (4)$$

with  $\mathbf{s}^{\text{up}} = (\mathbf{c}^{\text{up}})^{-1}$ . Positive viscous dissipation implies that the viscous compliance matrix is

positive-definite:  $s_{11}^{up} > 0$ ,  $s_{22}^{up} > 0$ ,  $s_{66}^{up} > 0$ , and  $s_{11}^{up}s_{22}^{up} - (s_{12}^{up})^2 > 0$ , which ensures that the compliance matrix is invertible. The viscous shear modulus  $G_{12}^{up}$  is defined as the ratio of shear stress to the engineering shear strain rate in the upright configuration:

$$G_{12}^{up} = \frac{1}{s_{66}^{up}} = c_{66}^{up} \quad (5)$$

Eqs. (3) and (4) involve 4 independent coefficients.

The number of independent coefficients decreases in the case of incompressibility (Destrade et al., 2002; Itskov and Aksel, 2002). Assuming virtual uniaxial tension tests in directions 1 and 2, the incompressibility constraint  $\dot{E}_{11} + \dot{E}_{22} = 0$  leads to the conditions

$$s_{11}^{up} + s_{12}^{up} = 0 \quad (6)$$

$$\text{and } s_{12}^{up} + s_{22}^{up} = 0. \quad (7)$$

The number of independent coefficients of the compliance matrix is thus reduced to two:

$$\mathbf{s}^{up} = \begin{pmatrix} s_{11}^{up} & -s_{11}^{up} & 0 \\ -s_{11}^{up} & s_{11}^{up} & 0 \\ 0 & 0 & s_{66}^{up} \end{pmatrix} \quad (8)$$

It also follows that the viscous compliance matrix is positive semi-definite (and thus singular) (Itskov and Aksel, 2002). The eigenvector associated with the vanishing eigenvalue corresponds to equibiaxial loading with zero dissipation rate.

Conducting the same two virtual experiments, but with the stress-strain relation expressed in terms of the stiffness matrix components leads to the two conditions

$$-c_{12}^{up} + c_{22}^{up} = 0 \quad (9)$$

$$c_{11}^{up} - c_{12}^{up} = 0 \quad (10)$$

$$\text{Thus } \mathbf{c}^{up} = \begin{pmatrix} c_{11}^{up} & c_{11}^{up} & 0 \\ c_{11}^{up} & c_{11}^{up} & 0 \\ 0 & 0 & c_{66}^{up} \end{pmatrix} \quad (11)$$

The stiffness matrix is also positive semi-definite. It also follows from incompressibility that

$$c_{11}^{up} = c_{22}^{up} = c_{12}^{up} = \infty. \text{ It is thus not possible to characterize two independent stiffness}$$

coefficients from the single matrix  $\mathbf{c}^{up}$ .

Compliance and stiffness matrices  $\mathbf{s}^\alpha$  and  $\mathbf{c}^\alpha$  resulting from a rotation of the coordinate

system by an angle  $\alpha$  around axis 3 can be derived from matrices  $\mathbf{s}^{up}$  and  $\mathbf{c}^{up}$  using the

transformation rules for tensors (Nye, 1957). Matrices  $\mathbf{s}^\alpha$  and  $\mathbf{c}^\alpha$  are full (i.e. normal and shear components of stress and strain tensors are coupled) except for the “tilt” orientation

$\alpha = \frac{\pi}{4}$ . This property follows from Eqs (6) to (11): indeed, denoting  $m = \cos \alpha$  and  $n = \sin \alpha$ ,

coefficients  $c_{16}^\alpha$ ,  $c_{26}^\alpha$ ,  $s_{16}^\alpha$  and  $s_{26}^\alpha$  write (Hearmon, 1961)

$$\begin{aligned} c_{16}^\alpha &= m^3 n (-c_{11}^{up} + c_{12}^{up} + 2c_{66}^{up}) + mn^3 (-c_{12}^{up} + c_{22}^{up} - 2c_{66}^{up}) \\ &\quad + (m^4 - 3m^2 n^2) c_{16}^{up} - (n^4 - 3m^2 n^2) c_{26}^{up} \\ c_{26}^\alpha &= mn^3 (-c_{11}^{up} + c_{12}^{up} + 2c_{66}^{up}) + m^3 n (-c_{12}^{up} + c_{22}^{up} - 2c_{66}^{up}) \\ &\quad + (m^4 - 3m^2 n^2) c_{26}^{up} - (n^4 - 3m^2 n^2) c_{16}^{up} \\ s_{16}^\alpha &= 2m^3 n \left( -s_{11}^{up} + s_{12}^{up} + \frac{1}{2} s_{66}^{up} \right) + 2mn^3 \left( -s_{12}^{up} + s_{22}^{up} - \frac{1}{2} s_{66}^{up} \right) \\ &\quad + (m^4 - 3m^2 n^2) s_{16}^{up} - (n^4 - 3m^2 n^2) s_{26}^{up} \\ s_{26}^\alpha &= 2mn^3 \left( -s_{11}^{up} + s_{12}^{up} + \frac{1}{2} s_{66}^{up} \right) + 2m^3 n \left( -s_{12}^{up} + s_{22}^{up} - \frac{1}{2} s_{66}^{up} \right) \\ &\quad + (m^4 - 3m^2 n^2) s_{26}^{up} - (n^4 - 3m^2 n^2) s_{16}^{up} \end{aligned} \quad (12)$$

which shows that, if  $\alpha = \frac{\pi}{4}$ , conditions  $c_{11}^{up} = c_{22}^{up}$  and  $c_{16}^{up} = c_{26}^{up} = 0$  yield  $c_{16}^{tilt} = c_{26}^{tilt} = 0$

whereas conditions  $s_{11}^{up} = s_{22}^{up}$  and  $s_{16}^{up} = s_{26}^{up} = 0$  yield  $s_{16}^{tilt} = s_{26}^{tilt} = 0$ . There thus exist four

orientations, spaced at  $45^\circ$  to each other, in which the stress and strain rate tensors are parallel to each other. This conclusion was reached previously by Wheeler using a different approach (Wheeler, 2010).

Coefficients  $c_{66}^\alpha$  and  $s_{66}^\alpha$  write

$$\begin{aligned} c_{66}^\alpha &= m^2 n^2 (c_{11}^{up} + c_{22}^{up} - 2c_{12}^{up}) + 2(m^3 n - n^3 m)(c_{26}^{up} - c_{16}^{up}) + (m^2 - n^2)^2 c_{66}^{up} \\ s_{66}^\alpha &= 4m^2 n^2 (s_{11}^{up} + s_{22}^{up} - 2s_{12}^{up}) + 4(m^3 n - n^3 m)(s_{26}^{up} - s_{16}^{up}) + (m^2 - n^2)^2 s_{66}^{up} \end{aligned} \quad (13)$$

which yields, if  $\alpha = \frac{\pi}{4}$ ,

$$\begin{aligned} c_{66}^{tilt} &= \frac{1}{4}(c_{11}^{up} + c_{22}^{up} - 2c_{12}^{up}) \\ s_{66}^{tilt} &= s_{11}^{up} + s_{22}^{up} - 2s_{12}^{up} = 4s_{11}^{up} \end{aligned} \quad (14)$$

The viscous shear moduli in the two orientations are

$$G_{12}^{tilt} = c_{66}^{tilt} = \frac{1}{s_{66}^{tilt}} = \frac{1}{4s_{11}^{up}} \quad (15)$$

$$\text{and } G_{12}^{up} = c_{66}^{up} = \frac{1}{s_{66}^{up}} = \frac{1}{4s_{11}^{tilt}}. \quad (16)$$

Noticeably,  $c_{66}^{tilt}$  is finite, which circumvents the indeterminacy of Eq. (14) arising from

$c_{11}^{up} = c_{22}^{up} = c_{12}^{up} = \infty$ . The macroscopic viscosity of a textured polycrystal is thus fully

characterized by the two coefficients  $G_{12}^{up}$  and  $G_{12}^{tilt}$ .

## 2.2. Micromechanics of NHC deformation

Let's  $\dot{\mathbf{u}}$  denote microscopic velocity and  $\mathbf{x}$  denote position vector. The grains are assumed to be rigid, i.e. the velocity difference between two points in the grain interior is null. The strain

rate tensor  $\dot{\varepsilon}_{ij} = \frac{1}{2} \left( \frac{\partial \dot{u}_i}{\partial x_j} + \frac{\partial \dot{u}_j}{\partial x_i} \right)$  is thus also null. Tractions on grain boundary,  $\mathbf{T}$ , are locally

balanced and are related to microscopic stress in grain interior according to Cauchy's law:

$$T_i = \sigma_{ij} n_j \quad (17)$$

where  $\mathbf{n}$  is an outward unit vector normal to grain boundary and summation over repeated indices is implied. The statistical representation of the microstructure via a single grain (Fig. 1) implies that tractions exerted locally on the grain boundary are balanced. Mechanical equilibrium requires that the stress tensor  $\boldsymbol{\sigma}$  is symmetric and that  $\nabla \cdot \boldsymbol{\sigma} = 0$ , which, via Eq. (17), implies as a corollary that the total force and moment resulting from tractions on grain boundary are null.

In a mono-component crystal, the force driving the lattice diffusion flux,  $\mathbf{J}_l$  (in units of volume per unit surface per unit time), is the gradient of the diffusion potential,  $\mu$ :

$$\mathbf{J}_l = -\frac{D_l}{kT} \nabla (\mu_A - \mu_V) = -\frac{D_l}{kT} \nabla \mu \quad (18)$$

where  $\mu_A$  and  $\mu_V$  are the chemical potential of atoms and vacancies (in units of energy per atom),  $k$  is Boltzmann's constant (in units of energy per atom and per Kelvin),  $T$  is the absolute temperature, and  $D_l$  is the lattice diffusion coefficient (in units of area per unit time) (Balluffi et al., 2005; Herring, 1950).  $D_l$  is the product of vacancy diffusion coefficient  $D_V$  and vacancy fraction  $X_V$ :  $D_l = D_V X_V$  (we will neglect the variation of  $X_V$  and treat  $D_l$  as a constant). On the grain boundary,  $\mu$  is related to the normal component of traction,  $T_n$ , by (Herring, 1950)

$$(\mu)_{\text{boundary}} = \mu^\circ - \Omega T_n \quad (19)$$

where  $\mu^\circ$  is a reference chemical potential and  $\Omega$  is the volume per atom. The NHC model is based on the hypotheses (i) that vacancy sources and sinks exist only at grain boundaries and

(ii) that these sources and sinks are perfect, i.e. that equilibrium vacancy concentration is maintained everywhere on grain boundaries. It follows from hypothesis (i) that, during quasi-steady-state deformation, the divergence of the flux  $\mathbf{J}_l$  vanishes,

$$\nabla \cdot \mathbf{J}_l = \frac{\partial J_l}{\partial x_i} = 0, \quad (20)$$

i.e. density remains uniform. Coupled with Eq. (18), this relation means that the chemical potential is harmonic,

$$\nabla^2 \mu = \frac{\partial}{\partial x_i} \left( \frac{\partial \mu}{\partial x_i} \right) = 0. \quad (21)$$

The model considers that the grain boundary consists of a thin layer of thickness  $\delta$  in which diffusion coefficient,  $D_b$ , is different from  $D_l$  (both having units of area per unit time). Inside this layer, the diffusion flux parallel to the grain boundary,  $\mathbf{j}_b$  (in units of volume per unit length per unit time) is related to the gradient of  $\mu$  as

$$\mathbf{j}_b = -\frac{\delta D_b}{kT} \nabla_s \mu = \frac{\delta D_b \Omega}{kT} \nabla_s T_n = \frac{\Omega \delta D_b}{kT} \frac{dT_n}{ds} \quad (22)$$

where  $\nabla_s$  denotes the gradient operator on the grain boundary surface and  $ds$  is an in-plane length increment on the grain boundary.

The representative grain is supposed to be in contact with an identical grain at each point on the ellipse surface (Fig. 1). The velocity jump at the boundary shared by grains centred at  $O$  and  $O'$  is denoted  $\Delta \dot{\mathbf{u}} = \dot{\mathbf{u}}_{O'} - \dot{\mathbf{u}}_O$  where  $\dot{\mathbf{u}}_O$  and  $\dot{\mathbf{u}}_{O'}$  are centroid velocities. The NHC model assumes that the velocity jump component normal to the boundary,  $\Delta \dot{u}_n$ , results only from the sum of the divergence of  $\mathbf{j}_b$  in the grain boundary and of the component of  $\mathbf{J}_l$  normal to grain boundary. As contact points are between identical grains having the same orientation (Fig. 1), the lattice diffusion flux  $\mathbf{J}_l$  is symmetric about grain boundary. Hence,

$$\Delta \dot{u}_n = 2(\mathbf{J}_l \cdot \mathbf{n})_{r=R} - \nabla_s \cdot \mathbf{j}_b. \quad (23)$$

In this paper, the two contributions to  $\Delta \dot{u}_n$  are considered separately. Their coupling has been analysed in three-dimension in Ref (Brassart and Delannay, 2019) based on a spherical representation of the grain: it was shown that the contribution of lattice diffusion is dominant if  $\delta D_b \ll R_G D_l$  whereas the contribution of grain boundary diffusion is dominant if  $\delta D_b \gg R_G D_l$ . For the tangential component of the velocity jump,  $\Delta \dot{u}_t$ , the NHC model assumes that it is related to the tangent component of the traction,  $T_t$ , by the linear law

$$T_t = \eta \Delta \dot{u}_t \quad (24)$$

where  $\eta$  (units of force per unit volume per unit time) is a boundary viscosity coefficient characterizing the sliding mechanism operating at microscopic scale.

Grain boundary curvature brings, between the two sides of the grain boundary, a diffusion potential difference  $\Delta \mu_\kappa = \gamma_b \kappa$  where  $\gamma_b$  is the grain boundary tension and  $\kappa$  is the curvature defined positive for a concave boundary.  $\Delta \mu_\kappa$  causes a migration velocity of the grain boundary in the normal direction,  $\dot{u}_{mn} = M_b \gamma_b \kappa$ , which is responsible for grain growth.  $\dot{u}_{mn}$  is not linked to macroscopic stress and strain rate. Gradients of  $\kappa$  imply gradients of  $\mu$ , which drive diffusion fluxes together with gradients of grain boundary migration. For an elliptical grain, these phenomena lead to a spontaneous decrease of the aspect ratio  $a/b$ . It is assumed that  $\gamma_b$  and  $M_b$  are low enough for allowing to consider that the evolution of  $a/b$  depends only on macroscopic stress and strain rate.

The micro-to-macro transition is achieved by identifying the macroscopic strain rate with the average microscopic strain rate,  $\langle \dot{\epsilon}_{ij} \rangle = \dot{E}_{ij}$ , and the macroscopic stress with the average



microscopic stress,  $\langle \sigma_{ij} \rangle = S_{ij}$ . Since the grain is rigid and all the deformation arises from interface phenomena, the following generalised definition of average strain is adopted:

$$\langle \dot{\epsilon}_{ij} \rangle = \frac{1}{2} \frac{1}{2V} \int_S (n_i \Delta \dot{u}_j + n_j \Delta \dot{u}_i) ds \quad (25)$$

where  $V$  is grain volume and the surface integral is carried out over the surface of the grain.

The first  $(1/2)$  factor accounts for the fact that the velocity jump occurs at the interface of two identical grains with the same volume. Conversely, an average of stress in the grain,  $\langle \sigma_{ij} \rangle$ , is defined from the traction field  $\mathbf{T}$  at grain boundary by the surface integral:

$$\langle \sigma_{ij} \rangle = \frac{1}{2V} \int_S (R_i T_j + R_j T_i) ds \quad (26)$$

Using Cauchy's law together with the divergence theorem and the condition of local mechanical equilibrium, it is readily shown that Eq. (26) is equivalent to the usual definition of  $\langle \sigma_{ij} \rangle$  as volume average stress.

### 2.3. Bounds for $G_{12}^{up}$ and $G_{12}^{tilt}$ via variational principles

The variational method rests on a kinematic principle and a statical principle (Brassart and Delannay, 2019). These principles invoke the concepts of admissible trial fields.

- In the kinematic principle, a trial velocity jump field at grain boundary,  $\Delta \dot{\mathbf{u}}$ , is admissible (i) if it is compatible with rigid grains and (ii) if Eq. (25) yields  $\langle \dot{\epsilon}_{ij} \rangle = \dot{E}_{ij}$ ; diffusion flux fields  $\mathbf{j}_b$  and  $\mathbf{J}_l$  are admissible if, given an admissible trial velocity jump field, they obey Eqs. (20) and (23).

- In the statical principle, a trial traction field  $\mathbf{T}$  at grain boundary is admissible (i) if it is equilibrated, and (ii) if Eq. (26) yields  $\langle \sigma_{ij} \rangle = S_{ij}$ ; a diffusion potential field  $\mu$  is admissible if, given an admissible trial traction field, Eq. (19) is obeyed on the grain boundary.

The trial velocity and diffusion flux fields yield an exact solution if the diffusion potential calculated from the constitutive Eqs (18) and (23) is continuous on the boundary, and if the traction field calculated from Eqs (19) and (24) is equilibrated. Conversely, trial boundary traction and diffusion potential fields yield an exact solution if the lattice diffusion flux calculated from the constitutive equation (18) is divergence free, and if the velocity jump field calculated from Eqs (23) and (24) is compatible with rigid grain.

For the kinematic trial velocity field respecting condition  $\langle \dot{\epsilon}_{ij} \rangle = \dot{E}_{ij}$ , we will opt for an affine field without grain translation and rotation. An affine field means that grain boundary velocity jumps are prescribed by macroscopic strain rate via

$$\Delta \dot{u}_i = 2\dot{E}_{ij}R_j \quad (27)$$

The absence of grain translation and rotation means that the antisymmetric part of the macroscopic velocity gradient tensor is taken to be null. The consequence of this choice of boundary conditions on the mechanical equilibrium, i.e. on the exactness of the solution, will be evaluated in Appendix 1. Conversely, for the choice of a statical trial velocity field respecting condition  $\langle \sigma_{ij} \rangle = S_{ij}$ , we will opt for the uniform stress field that consists in prescribing boundary tractions by macroscopic stress via

$$T_i = S_{ij}n_j \quad (28)$$

Uniform stress conditions do not forbid the existence of grain translation and/or rotation which

may be required by mechanical equilibrium (Appendix 1). We will discuss in Section 4.2 the realistic character of the use of these two types of boundary conditions for modelling the deformation of a random polycrystal.

The kinematic principle states that, among all admissible velocity and diffusion fields compatible with prescribed macroscopic strain rate, the actual exact fields minimise the functional

$$I = -\mathbf{S} : \dot{\mathbf{E}} + \Psi \quad (29)$$

where the first term represents the change in potential energy of the external loads and  $\Psi$  is a dissipation potential defined as:

$$\Psi = \frac{1}{V} \left[ \int_V \frac{kT}{2\Omega D_l} \mathbf{J}_l \cdot \mathbf{J}_l dv + \frac{1}{2} \int_S \left( \frac{kT}{2\Omega \delta D_b} \mathbf{j}_b \cdot \mathbf{j}_b + \frac{1}{2} \eta (\Delta \dot{u}_t)^2 \right) ds \right] = \Psi_l + \Psi_b + \Psi_{sl} \quad (30)$$

If the trial fields are the actual exact fields,  $\Psi$  is equal to half the power of dissipation in the body.  $\Psi$  acts as a potential for the macroscopic stress (Cocks, 1996), which is itself related to macroscopic deformation by the effective viscosity tensor. It follows that  $\Psi$  is related to macroscopic strain rate as

$$\Psi = \frac{1}{4} \dot{\mathbf{E}}_i \mathbf{C}_{ij}^+ \dot{\mathbf{E}}_j \quad (31)$$

where  $\mathbf{C}_{ij}^+$  is an apparent viscous stiffness matrix for which the superscript + is used because  $\Psi$  is larger than (half) the actual dissipation power in the body ( $i$  and  $j = 1, 2$ , or  $6$  and use is made of Nye's conventions for the definition of contracted stress and strain components). From Eq. (31), an upper bound (designated by superscript +) for the viscous shear modulus  $G_{12}$  is obtained as

$$G_{12}^+ = \frac{1}{2} \mathbf{C}_{66}^+ = \frac{1}{2} \frac{\Psi}{\dot{\mathbf{E}}_{12}^2} = \frac{1}{2} \frac{\Psi_l + \Psi_b + \Psi_{sl}}{\dot{\mathbf{E}}_{12}^2} \quad (32)$$

The statical principle states that, among all admissible trial stress fields and diffusion potential fields in equilibrium with a prescribed macroscopic stress, the actual exact fields minimise the functional

$$J = -\mathbf{S} : \dot{\mathbf{E}} + \Phi$$

where the dual dissipation potential is defined as:

$$\Phi = \frac{1}{V} \left[ \int_V \frac{D_l}{2\Omega kT} \nabla \mu \cdot \nabla \mu dv + \frac{1}{2} \int_S \left( \frac{\delta D_b}{2\Omega kT} \nabla_s \mu \cdot \nabla_s \mu + \frac{1}{2\eta} T_t^2 \right) ds \right] = \Phi_l + \Phi_b + \Phi_{sl} \quad (33)$$

If the trial fields are the actual exact fields,  $\Phi$  is equal to half the power of dissipation in the body.  $\Phi$  acts as a potential for the macroscopic strain rate (Cocks, 1996), which is itself related to macroscopic stress by the effective viscosity tensor. It follows that  $\Phi$  is related to macroscopic stress as

$$\Phi = \mathbf{S}_i \mathbf{S}_{ij}^+ \mathbf{S}_j \quad (34)$$

where, using again Nye's conventions,  $\mathbf{S}_{ij}^+$  is an apparent viscous compliance matrix for which the suffix + is used because  $\Phi$  is larger than (half) the actual dissipation power in the body.

From Eq. (34), a lower bound (designated by superscript -) for the viscous shear modulus  $G_{12}$  is obtained as

$$G_{12}^- = \frac{1}{2} \frac{1}{\mathbf{S}_{66}^+} = \frac{1}{2} \frac{\mathbf{S}_{12}^2}{\Phi} = \frac{1}{2} \frac{\mathbf{S}_{12}^2}{\Phi_l + \Phi_b + \Phi_{sl}} \quad (35)$$

The effective value of the viscous shear modulus will be denoted  $G_{12}$  without superscript. If boundary fields yield exact solutions,  $\Psi$  and  $\Phi$  are equal to half of the work power dissipation. The interest of the variational method is to allow the calculation of bounds for viscosity coefficients without having to solve the complete boundary-value problem, which may be intractable analytically. This is analogous to the bounds of Taylor and Sachs in crystal plasticity.



of vector  $\mathbf{R}$  connecting ellipse centroid to ellipse boundary are

$$\mathbf{R} = (b \sin \phi, a \cos \phi) \quad (36)$$

and the length is

$$R = \sqrt{b^2 \sin^2 \phi + a^2 \cos^2 \phi} = R_G B(\phi) \quad (37)$$

$$\text{where } B(\phi) = \sqrt{\frac{b}{a} + e \cos^2 \phi} \quad (38)$$

$$\text{with } e = \frac{a}{b} - \frac{b}{a}. \quad (39)$$

$\theta$  is related to  $\phi$  via

$$\tan \theta = \frac{R_1}{R_2} = \frac{b}{a} \tan \phi, \quad (40)$$

For integrals and derivatives along the perimeter of the ellipse, the curvilinear increment is

$$ds = \sqrt{\left(\frac{dR_1}{d\phi}\right)^2 + \left(\frac{dR_2}{d\phi}\right)^2} d\phi = R_G A(\phi) d\phi \quad (41)$$

$$\text{with } A(\phi) = \sqrt{\frac{a}{b} - e \cos^2 \phi} \quad (42)$$

The orientation of unit vectors normal and tangent to grain boundary is defined by angle  $\beta$  (Fig. 2):

$$\mathbf{n} = (\sin \beta, \cos \beta) \quad (43)$$

$$\mathbf{t} = (\cos \beta, -\sin \beta) \quad (44)$$

$\beta$  is linked to  $\phi$  and  $\theta$  via

$$\beta = \arctan\left(\frac{a}{b} \tan \phi\right) = \arctan\left[\left(\frac{a}{b}\right)^2 \tan \theta\right] \quad (45)$$

For the calculation of diffusion flux  $J_l$  and diffusion potential  $\mu$  in the case of dominance of lattice diffusion, use will be made, consistently with Eq. (36), of curvilinear coordinates  $\rho$  and  $\phi$  defined by expressing the position vector inside the ellipse as

$$\mathbf{x} = \rho \left( \sqrt{\frac{b}{a}} \sin \phi, \sqrt{\frac{a}{b}} \cos \phi \right) \quad (46)$$

for  $0 \leq \rho \leq \sqrt{ab} = R_G$ . For conciseness, the mathematical developments ensuing from this definition of curvilinear coordinates are detailed in the web document “Supplementary Material” joined to the paper (references to equations in Supplementary Material are preceded by letter A). In Sections 3.1.2 and 3.2.2, we focus only on the results ensuing from these developments.

### 3. Results

We consider pure shear loading with principal tensile direction oriented along  $\alpha$  with respect to axis  $2^{\text{up}}$  (Fig.2). For calculating the kinematic/upper bounds, macroscopic loading will be given by the strain rate tensor

$$\dot{\mathbf{E}} = \dot{E} \begin{bmatrix} -\cos 2\alpha & \sin 2\alpha \\ \sin 2\alpha & \cos 2\alpha \end{bmatrix} \quad (47)$$

Similarly, for calculating the statical/lower bounds, macroscopic loading will be given by stress tensor

$$\mathbf{S} = S \begin{bmatrix} -\cos 2\alpha & \sin 2\alpha \\ \sin 2\alpha & \cos 2\alpha \end{bmatrix}. \quad (48)$$

Equations will be developed for arbitrary  $\alpha$  values, and the bounds for  $G_{12}^{\text{up}}$  or  $G_{12}^{\text{tilt}}$  will be

obtained via Eqs. (32) and (35) using, respectively,  $\alpha = \frac{\pi}{4}$  and  $\alpha = 0$ . We will deal successively with the cases of dominance grain boundary diffusion ( $\delta D_b \gg R_G D_l$ ; case designated by subscript b) and of dominance of lattice diffusion ( $\delta D_b \ll R_G D_l$ ; case designated by subscript l).

### 3.1. Kinematic boundary conditions based on an affine velocity field

As detailed in the Supplementary Material, normal and tangent components of  $\Delta \dot{\mathbf{u}}$  are obtained from Eq. (27) as

$$\begin{aligned}\Delta \dot{u}_n &= \Delta \dot{\mathbf{u}} \cdot \mathbf{n} = 2R\dot{E} \cos(\theta + \beta - 2\alpha) \\ &= 2R_G \dot{E} \frac{1}{A(\phi)} (\cos 2\alpha \cos 2\phi + c \sin 2\alpha \sin 2\phi)\end{aligned}\quad (49)$$

$$\begin{aligned}\Delta \dot{u}_t &= \Delta \dot{\mathbf{u}} \cdot \mathbf{t} = 2R\dot{E} \sin(\theta + \beta - 2\alpha) \\ \text{and} \quad &= 2R_G \dot{E} \frac{1}{A(\phi)} (\sin 2\alpha \cos 2\phi - c \cos 2\alpha \sin 2\phi).\end{aligned}\quad (50)$$

$$\text{where } c = \frac{1}{2} \left( \frac{a}{b} + \frac{b}{a} \right) = \sqrt{1 + \left( \frac{e}{2} \right)^2}.\quad (51)$$

The contribution to  $\Psi$  due to grain boundary sliding,  $\Psi_{sl}$ , is easily calculated from  $\Delta \dot{u}_t$  (Eqs. (30) and (50)):



$$\begin{aligned}
\Psi_{sl} &= \frac{1}{V} \frac{1}{4} \eta \int_0^{2\pi} (\Delta \dot{u}_t)^2 ds \\
&= \dot{E}^2 R_G \eta \frac{1}{\pi} \left( \sin^2 2\alpha \int_0^{2\pi} \frac{\cos^2 2\phi}{A(\phi)} d\phi + c^2 \cos^2 2\alpha \int_0^{2\pi} \frac{\sin^2 2\phi}{A(\phi)} d\phi \right. \\
&\quad \left. + c \sin 4\alpha \int_0^{2\pi} \frac{\sin 2\phi \cos 2\phi}{A(\phi)} d\phi \right)
\end{aligned} \tag{52}$$

The three terms are elliptical integrals of the first kind.

### 3.1.1. $G_{12b}^{up+}$ and $G_{12b}^{tilt+}$ when grain boundary diffusion is dominant

If  $\delta D_b \gg R_G D_l$ , the contribution to  $\Delta \dot{u}_n$  due to  $\mathbf{J}_l$  in Eq. (23) can be neglected with respect to the contribution due to the divergence of the  $\mathbf{j}_b$ . Hence, via (Eq. (22))

$$\Delta \dot{u}_n = -\nabla_s \cdot \mathbf{j}_b = -\frac{dj_b}{ds} \tag{53}$$

The grain boundary flux is thus

$$\begin{aligned}
j_b &= -R_G \int_0^\phi \Delta \dot{u}_n(\phi') A(\phi') d\phi' \\
&= -R_G^2 \dot{E} \left[ \cos 2\alpha \sin 2\phi - c \sin 2\alpha \cos 2\phi + F_b(\alpha) \right]
\end{aligned} \tag{54}$$

where  $F_b(\alpha)$  is an integration constant. In order that the trial grain boundary flux field be as close as possible to the exact field, we calculate the value of  $F_b(\alpha)$  that corresponds to a minimum of the contribution due to grain boundary diffusion in the potential  $\Psi$ : Eq. (30) yields

$$F_b(\alpha) = -\frac{1}{\int_0^{2\pi} A(\phi) d\phi} \left( \cos 2\alpha \int_0^{2\pi} A(\phi) \sin 2\phi d\phi - c \sin 2\alpha \int_0^{2\pi} A(\phi) \cos 2\phi d\phi \right). \tag{55}$$

$F_b\left(\frac{\pi}{4}\right) \neq 0$ , whereas  $F_b(0) = 0$  as anticipated from symmetry.

According to Eq. (32),  $G_{12b}^+$  varies in proportion of the sum  $\Psi = \Psi_b + \Psi_{sl}$ . Denoting  $\eta_b$  the non-dimensional boundary viscosity coefficient

$$\eta_b = \frac{\Omega \delta D_b}{R_G^2 k T} \eta = \frac{D_b}{R_G^2} \eta, \quad (56)$$

Eqs (54) and (52) yield, for  $\alpha = \frac{\pi}{4}$ ,

$$G_{12b}^{up+} = \left( \frac{1}{8} \frac{1}{\pi} \int_0^{2\pi} A(\phi) \left( c \cos 2\phi - F_{b \frac{\pi}{4}} \right)^2 d\phi + \frac{1}{2} \eta_b \frac{1}{\pi} \int_0^{2\pi} \frac{\cos^2 2\phi}{A(\phi)} d\phi \right) \frac{R_G^3}{D_b}, \quad (57)$$

and for  $\alpha = 0$ ,

$$G_{12b}^{tilt+} = \left( \frac{1}{8} \frac{1}{\pi} \int_0^{2\pi} A(\phi) \sin^2 2\phi d\phi + \frac{1}{2} \eta_b c^2 \frac{1}{\pi} \int_0^{2\pi} \frac{\sin^2 2\phi}{A(\phi)} d\phi \right) \frac{R_G^3}{D_b}. \quad (58)$$

The first terms in Eqs. (57) and (58) are elliptical integrals of the second kind. It is shown in Appendix 1 that, except when  $a = b$ , the normal traction field corresponding to the boundary flux Eq. (54) is not equilibrated for  $\alpha = \frac{\pi}{4}$  as it brings a residual moment on the grain. Eq. (57)

is thus an upper bound for the exact  $G_{12b}^{up+}$ .

If grains are equiaxed, Eqs (57) and (58) become

$$G_{12b}^{tilt+} = G_{12b}^{up+} = G_{b_{equiaxed}}^+ = \left( \frac{1}{8} + \frac{1}{2} \eta_b \right) \frac{R_G^3}{D_b} \quad (59)$$

### 3.1.2. $G_{12l}^{up+}$ and $G_{12l}^{tilt+}$ when lattice diffusion is dominant

If  $\delta D_b \ll R_G D_l$ , the contribution to  $\Delta \dot{u}_n$  (Eq. (23)) due to the divergence of the  $\mathbf{j}_b$  can be neglected with respect to the contribution due to  $\mathbf{J}_l$ :

$$\frac{\Delta \dot{u}_n}{2} = \left( \mathbf{J}_l \cdot \mathbf{n} \right)_{r=R} \quad (60)$$

The mathematical developments yielding the solution for  $\mathbf{J}_l$  complying both with boundary condition Eq. (60) and with condition  $\nabla \cdot \mathbf{J}_l = 0$  (Eq. (20)) are presented in the Supplementary Material. In terms of components  $J_{ln}$  and  $J_{lt}$  in the directions normal and tangent to the boundary at  $\phi$ , the solution writes (Eqs. (A.22) and (A.23)) of Supplementary Material):

$$j_{ln} = \mathbf{J}_l \cdot \mathbf{n} = \rho \dot{E} \frac{1}{A(\phi)} (\cos 2\alpha \cos 2\phi + c \sin 2\alpha \sin 2\phi) \quad (61)$$

$$j_{lt} = \mathbf{J}_l \cdot \mathbf{t} = \rho \dot{E} \frac{1}{A(\phi)} (\sin 2\alpha \cos 2\phi - c \cos 2\alpha \sin 2\phi) + \rho A(\phi) \lambda(\alpha) \quad (62)$$

where  $\lambda(\alpha)$  is an arbitrary constant. Denoting  $\eta_l$  the non-dimensional boundary viscosity coefficient

$$\eta_l = \frac{\Omega D_l}{R_G k T} \eta = \frac{\mathcal{D}_l}{R_G} \eta = \frac{R_G}{\delta} \frac{D_l}{D_b} \eta_b, \quad (63)$$

$G_{12l}^{up+}$  and  $G_{12l}^{tilt+}$  then express as (Eqs (A.31) and (A.32) of Suppl. Mat.)

$$G_{12l}^{up+} = \left( \frac{1}{8} c + \frac{1}{2} \eta_l \frac{1}{\pi} \int_0^{2\pi} \frac{\cos^2 2\phi}{A(\phi)} d\phi \right) \frac{R_G^2}{\mathcal{D}_l} \quad (64)$$

$$G_{12l}^{tilt+} = \left( \frac{1}{8} c + \frac{1}{2} \eta_l c^2 \frac{1}{\pi} \int_0^{2\pi} \frac{\sin^2 2\phi}{A(\phi)} d\phi \right) \frac{R_G^2}{\mathcal{D}_l} \quad (65)$$

Quite remarkably, the first term, i.e. the contribution due to diffusion, is the same for  $\alpha = \frac{\pi}{4}$

and  $\alpha = 0$ . However, as shown in Appendix 1, the boundary traction field corresponding to Eq.

(61) is not equilibrated when  $\alpha = \frac{\pi}{4}$ , except when  $a = b$ . Eq. (64) is thus an upper bound for

the exact  $G_{12l}^{up+}$ . Nevertheless, Eqs. (64) and (65) indicate that, when lattice diffusion

dominates, viscosity anisotropy arises essentially from grain boundary sliding.

If grains are equiaxed ( $a = b$ ), shear viscosity reduces to

$$G_{12l}^{tilt+} = G_{12l}^{up+} = G_{l_{equiaxed}}^{+} = \left( \frac{1}{8} + \frac{1}{2} \eta_l \right) \frac{R_G^2}{D_l} \quad (66)$$

The expressions look thus identical for  $G_{b_{equiaxed}}^{+}$  and  $G_{l_{equiaxed}}^{+}$ .

### 3.2. Statical boundary conditions based on a uniform stress field

As detailed in the Supplementary Material (Eqs. (A.37) and (A.38)) normal and tangent components of  $\mathbf{T}$  are then obtained from Eq. (28) as

$$\begin{aligned} T_n &= \mathbf{T} \cdot \mathbf{n} \\ &= S \cos(2\alpha - 2\beta) = S \frac{1}{A^2(\phi)} \left[ \cos 2\alpha \left( c \cos 2\phi - \frac{e}{2} \right) + \sin 2\alpha \sin 2\phi \right] \end{aligned} \quad (67)$$

$$\begin{aligned} T_t &= \mathbf{T} \cdot \mathbf{t} \\ &= S \sin(2\alpha - 2\beta) = -S \frac{1}{A^2(\phi)} \left[ \cos 2\alpha \sin 2\phi - \sin 2\alpha \left( c \cos 2\phi - \frac{e}{2} \right) \right] \end{aligned} \quad (68)$$

Mathematical details for the computation of the statical solutions are provided in the

Supplementary Material. It is shown in Appendix 1 that, when  $\alpha = \frac{\pi}{4}$ , the normal traction field

Eq.(67) brings a rotation velocity of the grain, except when  $a = b$ .

When grain boundary diffusion is dominant, the solutions express by Eqs. (A.47) and (A.48) of

Suppl. Mat.: for  $\alpha = \frac{\pi}{4}$ ,

$$\frac{1}{G_{12b}^{up-}} = \left[ \frac{2}{\pi} \int_0^{2\pi} \frac{\cos^2 2\phi}{A^9(\phi)} \left( A^2(\phi) - \frac{e \sin^2 2\phi}{2 \cos 2\phi} \right)^2 d\phi + \frac{1}{2} \frac{1}{\eta_b} \frac{1}{\pi} \int_0^{2\pi} \frac{\left( c \cos 2\phi - \frac{e}{2} \right)^2}{A^3(\phi)} d\phi \right] \frac{D_b}{R_G^3} \quad (69)$$

and for  $\alpha = 0$ ,

$$\frac{1}{G_{12b}^{tilt-}} = \left( \frac{2}{\pi} \int_0^{2\pi} \frac{\sin^2 2\phi}{A^9(\phi)} d\phi + \frac{1}{2} \frac{1}{\eta_b} \frac{1}{\pi} \int_0^{2\pi} \frac{\sin^2 2\phi}{A^3(\phi)} d\phi \right) \frac{\mathcal{D}_b}{R_G^3}. \quad (70)$$

If grains are equiaxed ( $a = b$ ), Eqs (69) and (70) become

$$G_{12b}^{tilt-} = G_{12b}^{up-} = G_{b_{equiaxed}}^- = \left( 2 + \frac{1}{2} \frac{1}{\eta_b} \right)^{-1} \frac{R_G^3}{\mathcal{D}_b}. \quad (71)$$

When lattice diffusion is dominant, the two solutions express by Eqs. (A.72) and (A.73) :

$$\begin{aligned} \frac{1}{G_{12l}^{up-}} = & \left\{ \frac{1}{\pi} \int_0^{2\pi} \left[ \frac{\sin^2 2\phi}{A^2(\phi)} + \frac{B^2(\phi)}{A^8(\phi)} \cos^2 2\phi \left( A^2(\phi) - \frac{e \sin^2 2\phi}{2 \cos 2\phi} \right)^2 \right. \right. \\ & \left. \left. + \frac{1}{2} e \frac{\sin 4\phi \sin 2\phi}{A^6(\phi)} \left( A^2(\phi) - \frac{e \sin^2 2\phi}{2 \cos 2\phi} \right) \right] d\phi + \frac{1}{2} \frac{1}{\eta_l} \frac{1}{\pi} \int_0^{2\pi} \frac{\left( c \cos 2\phi - \frac{e}{2} \right)^2}{A^3(\phi)} d\phi \right\} \frac{\mathcal{D}_l}{R_G^2} \end{aligned} \quad (72)$$

and

$$\begin{aligned} \frac{1}{G_{12l}^{tilt-}} = & \left\{ \frac{1}{\pi} \int_0^{2\pi} \left[ \left( \frac{c \cos 2\phi - \frac{e}{2}}{A(\phi)} + A(\phi) \gamma^{tilt} \right)^2 + \frac{B^2(\phi)}{A^8(\phi)} \sin^2 2\phi \right. \right. \\ & \left. \left. - e \frac{\sin^2 2\phi}{A^5(\phi)} \left( \frac{c \cos 2\phi - \frac{e}{2}}{A(\phi)} + A(\phi) \gamma^{tilt} \right) \right] d\phi + \frac{1}{2} \frac{1}{\eta_l} \frac{1}{\pi} \int_0^{2\pi} \frac{\sin^2 2\phi}{A^3(\phi)} d\phi \right\} \frac{\mathcal{D}_l}{R_G^2} \end{aligned} \quad (73)$$

with, according to Eq. (A.68)

$$\gamma^{tilt} = - \frac{\int_0^{2\pi} \left( c \cos 2\phi - \frac{e}{2} - \frac{1}{2} e \frac{\sin^2 2\phi}{A^4(\phi)} \right) d\phi}{\int_0^{2\pi} A^2(\phi) d\phi} \neq 0 \quad (74)$$

In contrast to  $G_{12l}^+$ , anisotropy of  $G_{12l}^-$  arises from both lattice diffusion and grain boundary

sliding. If grains are equiaxed ( $a = b$ ), these results reduce to

$$G_{12l}^{tilt-} = G_{12l}^{up-} = G_{l_{equiaxed}}^{-} = \left( 2 + \frac{1}{2} \frac{1}{\eta_l} \right)^{-1} \frac{R_G^2}{\mathcal{D}_l}. \quad (75)$$

### 3.3. Comparison of kinematic and statical bounds

Figures 3 and 4 illustrate the effect of the increase of the ellipse aspect ratio on the dependence on  $\eta$  of the kinematic and statical bounds for the cases of grain boundary diffusion ( $G_{12b}^{up}$ ,  $G_{12b}^{tilt}$  : Figs. 3a and 3b) and lattice diffusion ( $G_{12l}^{up}$ , and  $G_{12l}^{tilt}$  : Figs. 4a and 4b). The curves are drawn for  $a/b = 1$ , (black), 2 (red), and 3 (blue). According to Eq. (2),  $a/b = 2$  and 3 correspond to total strain  $E = 0.35$  and  $E = 0.55$ , respectively. Being proportional to the sum  $\Psi_b + \Psi_{sl}$  (Eq. (32)), kinematic bounds increase linearly with  $\eta_b$  and  $\eta_l$ , respectively. The straight lines (continuous) are thus  $G_{12b}^{+}$  and  $G_{12l}^{+}$  whereas the curves (dashed) are the statical bounds  $G_{12b}^{-}$  and  $G_{12l}^{-}$ . It can be noticed on Fig. 4, that  $G_{12l}^{tilt+}$  and  $G_{12l}^{up+}$  are identical at  $\eta = 0$  (Eqs. (64) and (65)). In accordance with the concept of variational bounds, statical bounds are always lower than kinematic bounds.

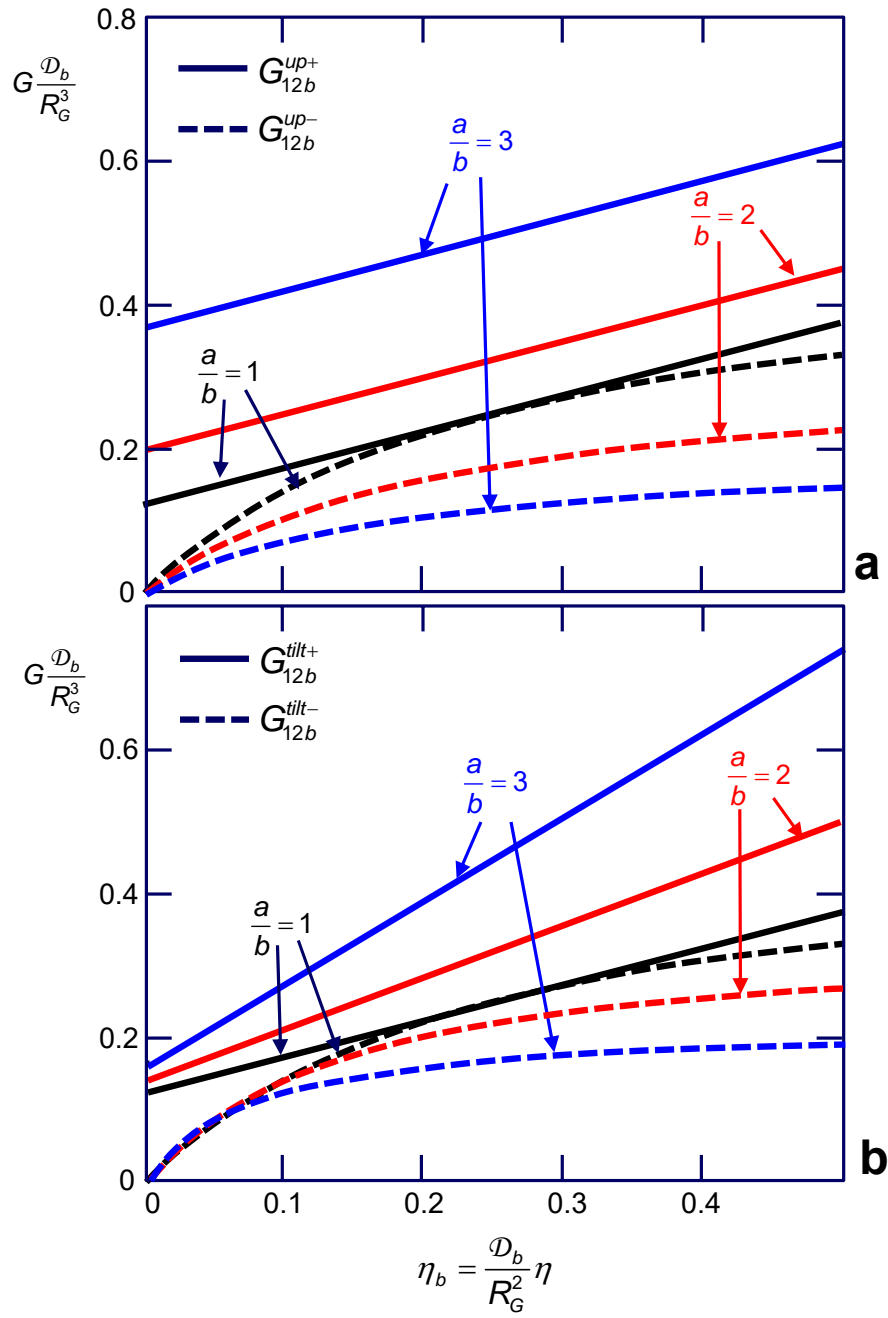


**Figure 3:** Grain boundary diffusion: dependence on boundary viscosity coefficient  $\eta$  of the upper and lower bounds for (a)  $G_{12b}^{up}$  and (b)  $G_{12b}^{tilt}$  for  $a/b = 1, 2$ , and  $3$ .

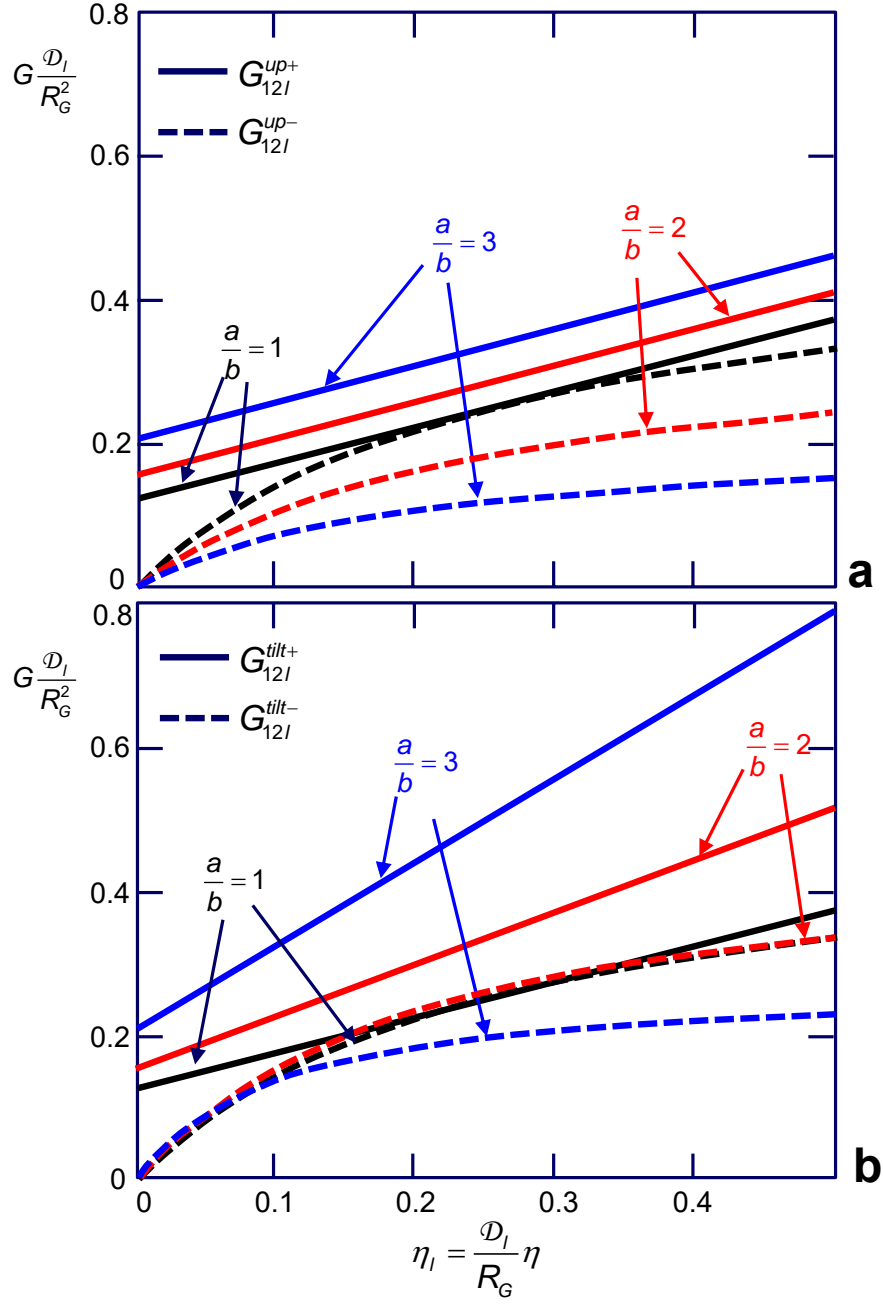


**Figure 4:** Lattice diffusion: dependence on  $\eta$  of the upper and lower bounds for (a)  $G_{12I}^{up}$  and (b)

$G_{12I}^{tilt}$  for  $a/b = 1, 2$ , and  $3$ .



## 4. Discussion

### 4.1. Equiaxed grains

The black lines drawn in Figs. 3 and 4 for  $G_{b_{\text{equiaxed}}}^+$  and  $G_{l_{\text{equiaxed}}}^+$  (Eqs. (59) and (66)) and for

$G_{b_{\text{equiaxed}}}^-$  and  $G_{l_{\text{equiaxed}}}^-$  (Eqs. (71), and (75)) are reproduced on common axes in Figure 5. A point

of tangency is observed when  $\eta_b$  or  $\eta_l = 0.25$ , which, in both cases, corresponds to the

boundary viscosity value  $\eta^* = \frac{G}{R_G}$ . It can be verified that, when  $\eta = \eta^*$ , stress uniformity

brings affine deformation, and reciprocally. The demonstration was developed in Appendix C of Ref. (Brassart and Delannay, 2019) for the case a spherical grain, for which the two bounds presented a similar point of tangency (the expressions of the bounds for a sphere are given in Table 1 of the latter reference). The agreement between the two solutions (which, as shown in Appendix 1, are both exact for equiaxed grains) when  $\eta = \eta^*$  attests for the validity of the mathematical procedure developed for calculating the two bounds. It is shown in Appendix 2 that the affine bound and the uniform stress bound are the two sole exact solutions that are possible for a circular cylinder.

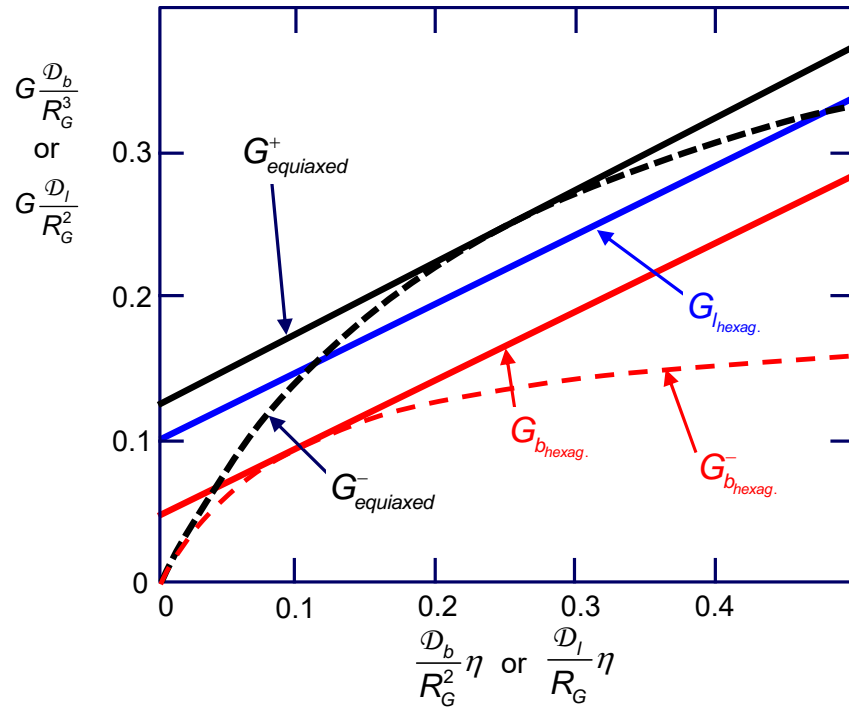


**Figure 5:** Dependence on  $\eta$  of the kinematic and statical solutions,  $G^+_{equiaxed}$  (continuous black) and  $G^-_{equiaxed}$  (dashed black), for the two diffusion modes (Eqs. (59), (66), (71), and (75)) together with the kinematic solutions for a hexagonal lattice of grains,  $G_{bhexag.}$  (red) and  $G_{lhexag.}$  (blue) (Eqs. (78) and (79)), and the statical solution for a hexagonal grain,  $G^-_{bhexag.}$  (Eq. (80)).

The kinematic bounds for equiaxed grains (Eqs. (59) and (66)) can be compared with the solutions reported by Mori et al (Mori et al., 1998b), Onaka et al (Onaka et al., 1998), Takei and Holtzman (Takei and Holtzman, 2009) and Rudge (Rudge, 2018), who also used a 2D model considering a grain with circular cross-section together with affine grain velocity. For  $\eta_b = 0$ , Eq. (59) is identical to the result obtained by Takei and Holtzman and by Rudge assuming zero boundary viscosity. Mori et al and Onaka et al analysed the evolution of strain rate through transient state and steady state. Their results for the steady-state creep rate also agree with the present results: equation (27) of (Mori et al., 1998b) yields an expression for the steady-

state  $G_l$  which is identical to the present Eq. (66) ; equation (40) of (Mori et al., 1998b) and equation (58) of (Onaka et al., 1998) yield an expression for steady state  $G_b$  equal the present Eq. (59) (accounting for the factor two difference in the definition by the authors of the boundary thickness  $\delta$ ).

A two-dimensional periodic lattice with hexagonal symmetry also presents in-plane isotropic properties (Nye, 1957). In a periodic lattice, grain displacements are affine by construction. For a periodic lattice of hexagonal grains, the creep rate under zero boundary viscosity ( $\eta = 0$ ) has been calculated by Spingarn and Nix (Spingarn and Nix, 1978) for the case of grain boundary diffusion, and by Rudge (Rudge, 2018) for the case of lattice diffusion. Reference to Eqs (59) and (66) with  $\eta = 0$  reveals the differences between the present results and the results of these authors:

$$G_{\text{Spingarn Nix}} = \frac{1}{144} \left( \frac{2\pi}{\sqrt{3}} \right)^{\frac{3}{2}} \frac{R_G^3}{D_b} = \frac{1}{20.8} \frac{R_G^3}{D_b} < \left( G_{b_{\text{equiaxed}}}^+ \right)_{\eta=0} = \frac{1}{8} \frac{R_G^3}{D_b} \quad (76)$$

$$G_{\text{Rudge}} = \frac{1}{9.9} \frac{R_G^2}{D_l} < \left( G_{l_{\text{equiaxed}}}^+ \right)_{\eta=0} = \frac{1}{8} \frac{R_G^2}{D_l} \quad (77)$$

The viscosity of a hexagonal lattice is thus lower than the kinematic prediction of the model based on a circular grain. The difference is larger in the case of grain boundary diffusion. For the latter case, Kim et al (Kim et al., 2004) have calculated the evolution of viscosity during deformation of a periodic array of initially hexagonal grains while accounting for boundary viscosity ( $\eta \neq 0$ ). At the onset of deformation i.e. for regular hexagons, Eq. 11 of Ref. (Kim et al., 2004) translates, accounting for our notations, into

$$G_{b_{\text{hexag.}}} = \frac{1}{144} \left( \frac{2\pi}{\sqrt{3}} \right)^{\frac{3}{2}} \left( 1 + 36 \left( \frac{2\pi}{\sqrt{3}} \right)^{-1} \eta_b \right) \frac{R_G^3}{D_b} = \left( \frac{1}{20.8} + \frac{1}{2.1} \eta_b \right) \frac{R_G^3}{D_b} \quad (78)$$

The first term is thus identical to the solution of Spingarn and Nix (Eq.(76)). The slope 1/2.1 is only very slightly lower than the slope 1/2 of  $G_{b_{equiaxed}}^+$  (Eq. (59)). As the contribution of boundary viscosity is the same for lattice diffusion as for grain boundary diffusion, the result of (Rudge, 2018) may be extended as

$$G_{l_{hexag.}} = \left( \frac{1}{9.9} + \frac{1}{2.1} \eta_l \right) \frac{R^2}{D_b} \quad (79)$$

The straight lines corresponding to Eqs. (78) and (79) are plotted in Fig. 5 for comparison with Eqs. (59) and (66). It can be argued that (Eqs. (59) and (66)) should be corrected for accounting for the fact that, in a random arrangement of grains with average coordination equal to six, the average distance between grain centroids is the distance between centroids in a regular lattice of hexagons with area  $\pi R_G^2$ . This distance is somewhat smaller than the diameter  $2R_G$  of the equivalent circle. This difference brings diffusion fluxes to be larger for a circular grain. In the case of grain boundary diffusion, the effect of this difference is expected to be partly compensated by the shorter length of the integration path along the boundary. The correction would thus be small. Anyway, Fig. 5 shows that the correction to be made to bring  $G_{equiaxed}^+$  (which is exact for a circular grain) to agree with  $G_{b_{hexag.}}$  or  $G_{l_{hexag.}}$  (which are exact for a hexagonal grain) does not merely amount to a change of the reference length.

The effect of grain rotation on the viscosity of hexagonal lattices under dominance of grain boundary diffusion has been analysed by Kim et al (Kim et al., 2009) for the a regular lattice and by Wheeler (Wheeler, 2010) for lattices of deformed hexagons with variable aspect ratio (in a periodic lattice, translational symmetry implies that the rotation velocity vector is identical in all grains). These authors consider infinite grain boundary mobility. They show that, in a regular lattice, grain rotation does not modify viscosity, i.e. Eq. (78) remains valid whatever the grain

rotation velocity: Eq. (78) is identical to Eq. (19) in Ref. (Kim et al., 2009), which agrees with Eq. 39 in (Wheeler, 2010). This means that, overall, the relative contributions of boundary diffusion and boundary sliding remain unchanged. This is consistent with the observation of Wheeler that, whatever the boundary viscosity  $\eta$ , the grain rotation velocity coupled to strain rate is indeterminate for a regular lattice (Wheeler, 2010).

Fig. 5 also presents the curve, dotted in red and denoted  $G_{b_{hexag}}^-$ , that is obtained if the Coble viscosity of a regular hexagonal grain not embedded in a regular lattice is calculated by applying uniform stress boundary conditions instead of affine boundary conditions:

$$G_{b_{hexag}}^- = \left( \frac{\pi}{2\sqrt{3}} \right)^{\frac{3}{2}} \left( \frac{9}{2} + \frac{1}{\eta_b} \frac{1}{4} \frac{\pi}{\sqrt{3}} \right)^{-1} \frac{R_G^3}{D_b} \quad (80)$$

The mathematics for calculating this result are presented in the Supplementary Material (Eq.

(A.97)). Similarly to curve  $G_{b_{equiaxed}}^-$  with respect to line  $G_{b_{equiaxed}}^+$ , curve  $G_{b_{hexag}}^-$  is lower than the

affine line  $G_{b_{hexag}}$  (Eq. (78)), with a point of tangency at  $\eta_b = \frac{\pi}{18\sqrt{3}}$ . This point corresponds to

the condition  $\eta = \eta_{hexag}^* = \frac{G}{H}$  where  $H$  is the distance from grain centroid to grain facet. Like

for the circular grain, this condition corresponds to the coexistence of stress uniformity and affine grain velocities.

For grain boundary diffusion, the large difference between the predictions derived when considering a circular grain or a hexagonal lattice of grains ensues from a fundamental difference between the two models. This difference is conspicuous when comparing the variation of the normal traction field,  $T_n$ , along the perimeter of the grain. In the hexagonal lattice model, continuity of the diffusion potential implies that  $T_n$  is zero at all vertices

(Wheeler, 2010). It follows a discontinuity of the gradient  $\frac{dT_n}{ds}$  at the vertex, i.e. different diffusion fluxes on the two faces, which in turn implies the existence of a diffusion flux along the grain boundary exiting the hexagon. In the circular grain model, whatever the boundary conditions, the normal traction fields  $T_n$  varies monotonously along the grain boundary, which implies the continuity of the diffusion flux, i.e. no flux exchange with surrounding grains. The contribution of diffusional fluxes along external grain boundaries was pointed out by Rudge (Rudge, 2018) who showed that, for a hexagonal grain, suppression of diffusion fluxes along external boundaries brings the viscosity for  $\eta = 0$  to be much closer to the viscosity calculated for a circular grain. Hence, actually, the circular grain model is not compatible with the hypotheses underlying Coble creep. Incidentally, this is true also for the spherical grain model, of which Coble made use in his pioneering paper based on an analogy with Herring's model for Nabarro-Herring creep (Coble, 1963; Herring, 1950)). In the case of lattice diffusion, the diffusional exchanges of a hexagonal grain with surrounding grains are more similar to the case of a circular grain (Eq. (79)).

#### 4.2. *Realistic character of boundary conditions*

Before discussing the case of elongated grains, we address the question of whether the two types of boundary fields are realistic, i.e. are close enough to the actual velocity jump field and traction field at grain boundaries in a random polycrystal.

As mentioned already, the affine velocity field is exact by construction in a periodic lattice of grains (which does not preclude an identical rotation velocity of all the grains (Kim et al., 2009; Wheeler, 2010)). It can be anticipated that, with respect to a periodic lattice, the average

velocity field in a random polycrystal is not very largely modified by the departure from periodicity and the occurrence of grain rotation. The kinematic boundary field based on an affine velocity field without grain rotation can thus a priori be considered realistic for a random polycrystal.

The situation is different for the uniform stress boundary field. The latter is obviously not realistic for a periodic lattice of grains as the stress field in such a lattice (in which grain displacements are affine) is generally very far from uniform (Kim et al., 2004; Spingarn and Nix, 1978). This is the reason why uniform stress boundary conditions have not been considered in previous literature for modelling a random polycrystal. Nevertheless, it has been shown in Section 4.1 that, when equiaxed grains are represented by a circular cylinder or a regular hexagon, stress uniformity and affine displacement of the grains coexist when  $\eta = \eta^*$ . Hence, when  $a/b = 1$ , the uniform stress boundary field is as realistic as the affine boundary field when  $\eta$  is close to  $\eta^*$ . Figs 3 and 4 show that, when  $a/b > 1$ , kinematic lines and statical curves present no point of tangency, i.e. stress uniformity and affine displacement of the grains never coexist when  $a/b > 1$ . However, there always exists a particular  $\eta$  value (which we again denote  $\eta^*$ ) at which the gap between the two bounds is minimum, i.e. at which the difference between the uniform stress field and the affine velocity field is minimum. This gap increases when aspect ratio increases. It may thus be guessed that, when  $\eta = \eta^*$ , the average field in a random polycrystal with elongated grains is close to an average between a uniform stress field and an affine velocity field. But, as the affine field is expected to be close to the actual average field in a random polycrystal whatever  $\eta$ , the strong increase of the difference between the two bounds when the difference  $\|\eta - \eta^*\|$  increases implies a strongly increasing departure of the actual average field from a uniform stress field.

It is thus concluded that, unless  $\eta$  is close to  $\eta^*$ , the upper (affine) bound is a much more realistic estimate for the effective viscosity of a random 2D polycrystal than the lower (uniform stress) bound (like the Taylor hypothesis in crystal plasticity provides a better estimate of the plastic anisotropy of a polycrystal than the Sachs hypothesis). For a periodic lattice of grains, the affine bound is the exact solution whatever the aspect ratio. Relaxation of dissipation with respect to this bound may be possible in a random polycrystal owing to the departure from periodicity. In addition, when  $a/b > 1$ , relaxation with respect to the bound  $G_{12}^{up+}$  may result from grain rotation ( $G_{12}^{tilt+}$  does not involve grain rotation).

For a polycrystal with equiaxed grains, no relaxation from the affine bound is expected to be possible when  $\eta = \eta^*$  because the kinematic bound and the statical bound then merge into a single solution. The following question is how much does, in such a polycrystal, the effective  $G_{equiaxed}$  differ from  $G_{equiaxed}^+$  when  $\eta \neq \eta^*$ . For the case of grain boundary diffusion, an answer to that question can be found in the work of Wei et al (Wei et al., 2008) who carried out 2D simulations by the finite element method (FEM) of the Coble deformation of a numerically generated random polycrystal with (more or less) equiaxed grains (figure 4a in the reference). Fig. 6 reproduces figure 5a of (Wei et al., 2008): the blue squares are their numerical results for the variation of the steady-state viscosity with boundary viscosity  $\eta$  (the labels on the axes have been converted to correspond to the notations of the present paper). The red curve added on the figure is the curve  $G_{b_{hexag.}}$  drawn according to Eq. (78) using the average grain size reported by the authors (the position of the curve may have to be shifted depending on the value chosen for this average). The agreement between Eq. (78) and FEM results is excellent, which shows that the random character of the model does not bring about a significant relaxation with



respect to purely affine deformation (the authors have not reported the amplitude of random grain rotations in their numerical model).

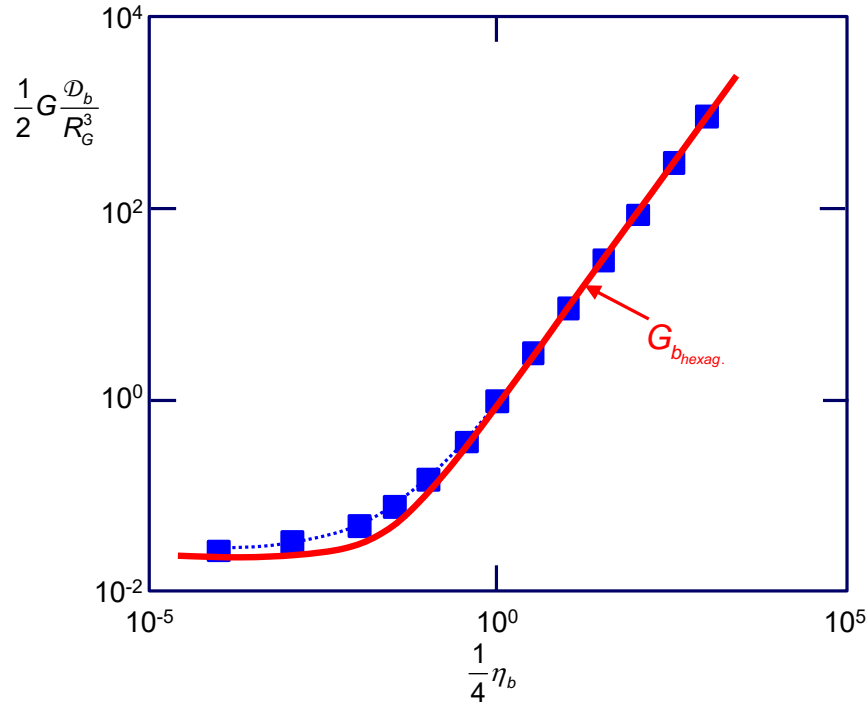


**Figure 6:** Comparison of the curve  $G_{b_{hexag.}}$  drawn according to Eq. (78) with FEM simulations of a random 2D polycrystal (Wei et al., 2008)

The reason why the uniform stress boundary field is not realistic (unless  $\eta$  is close to  $\eta^*$ ) is related to the fact that the uniform stress hypothesis implies the hypothesis that normal and tangent components of boundary tractions,  $T_n$  and  $T_t$ , can vary independently of one another. This hypothesis is not correct:  $T_n$  is linked to  $\Delta \dot{u}_n$ ,  $T_t$  is linked to  $\Delta \dot{u}_t$ , and  $\Delta \dot{u}_n$  and  $\Delta \dot{u}_t$  are in turn linked by the constraint of compatibility of deformation of adjacent grains.  $T_n$  and  $T_t$  are thus coupled. In other words, diffusion and grain boundary sliding are processes that act in series, not in parallel. The restriction on the realistic character of the uniform stress field was not raised by the authors in their recent paper (Brassart and Delannay, 2019). A particular

consequence is that the derivation of a size sensitivity exponent on the basis of the statical bound is not fully meaningful.

#### 4.3. Elongated grains

In the case of elongated grains,  $G_{12}^{tilt+}$ ,  $G_{12}^{tilt-}$ , and  $G_{12l}^{up-}$  are exact solutions, whereas  $G_{12l}^{up+}$  is not exact (Appendix 1). Yet,  $G_{12}^{tilt+}$ ,  $G_{12}^{tilt-}$  are not identical when  $\eta = \eta^*$ . This gap between the two bounds at  $\eta = \eta^*$  (Figs 3 and 4) suggests that departure from periodicity may bring about relaxation with respect to the affine/upper bounds (relaxation with respect to  $G_{12}^{up+}$  may also be due to grain rotation). The actual average velocity field being close to affine, it can be guessed that the dependence on  $\eta$  of the effective  $G_{12}^{up}$  and  $G_{12}^{tilt}$  does not much depart from a straight line. We can postulate that, in Figs 3 and 4, these dependences on  $\eta$  would be represented by straight lines located inside the gap between the two bounds. We assume that, for  $\eta = \eta^*$ , the relative departure from  $G_{12}^{up}$  and  $G_{12}^{tilt}$  is the same for the two bounds. A closer estimate for  $G_{12}^{up}$  and  $G_{12}^{tilt}$  can then be obtained by correcting the two bounds using a factor,  $f$ , such that the corrected kinematic bound is brought to have a point of tangency with the corrected statical bound: for example, the estimate for the effective  $G_{12}^{up}$  is

$$G_{12}^{up} = fG_{12}^{up+}, \quad (81)$$

where  $f$  is such that the line  $fG_{12}^{up+}$  is tangent to the curve  $\frac{G_{12}^{up-}}{f}$ . The factor  $f$  can easily be

derived from the equations for  $G_{12}^{+}$  and  $G_{12}^{-}$  given in Section 3. This estimate for the effective

$G_{12}^{up}$  and  $G_{12}^{tilt}$  thus requires the knowledge of the variation of the statical bounds in a range of  $\eta$  values around  $\eta = \eta^*$ .

Owing to the gap between lines  $G_{12}^+$  and curves  $G_{12}^-$ , the mere observation of Figs 3 and 4 does not allow to ascertain whether grain elongation causes hardening or softening. Experimentally, creep tests are conducted under uniaxial loading. In the direction of grain elongation, the evolution of the uniaxial creep rate,  $\dot{E}$ , normalized with respect to its initial value,  $\dot{E}_{uniaxed}$ , is, according to Eqs. (15) and (16), represented by the evolution of the ratio

$$\frac{\dot{E}}{\dot{E}_{uniaxed}} = \frac{s_{11}^{up}}{s_{11equiaxed}} = \frac{G_{eqiaxed}}{G_{12}^{tilt}}. \text{ The existence of a strain hardening effect is assessed in Fig. 7:}$$

the curves drawn in black present, for the two types of diffusion paths and for  $\eta_b = \eta_l = 0$  (Fig.

7a) or  $\eta_b = \eta_l = 0.4$  (Fig. 7b), the evolution with strain,  $E$ , of the ratio  $\frac{G_{eqiaxed}}{G_{12}^{tilt}}$  where  $G_{12}^{tilt}$  is the

effective viscosity estimated according to the procedure described above. For comparison, the

curves drawn in red are the ratio  $\frac{G_{eqiaxed}}{G_{12}^{tilt+}}$  where  $G_{12}^{tilt+}$  is the kinetic bound. Except curves

$\frac{G_{beqiaxed}}{G_{b12}^{tilt}}$  (grain boundary diffusion) with  $\eta_b = \eta_l = 0$  (Fig. 7a), Fig. 7 attests for a strain hardening

effect, which is larger for lattice diffusion than for grain boundary diffusion and increases when

$\eta$  increases. Owing to the correction factor  $f$  (Eq. (81)), the strain hardening effect is much

weaker for  $\frac{G_{eqiaxed}}{G_{12}^{tilt}}$  than for  $\frac{G_{eqiaxed}}{G_{12}^{tilt+}}$ : curve  $\frac{G_{beqiaxed}}{G_{b12}^{tilt}}$  even exhibits strain softening when  $\eta_b =$

$\eta_l = 0$  (Fig. 7a).

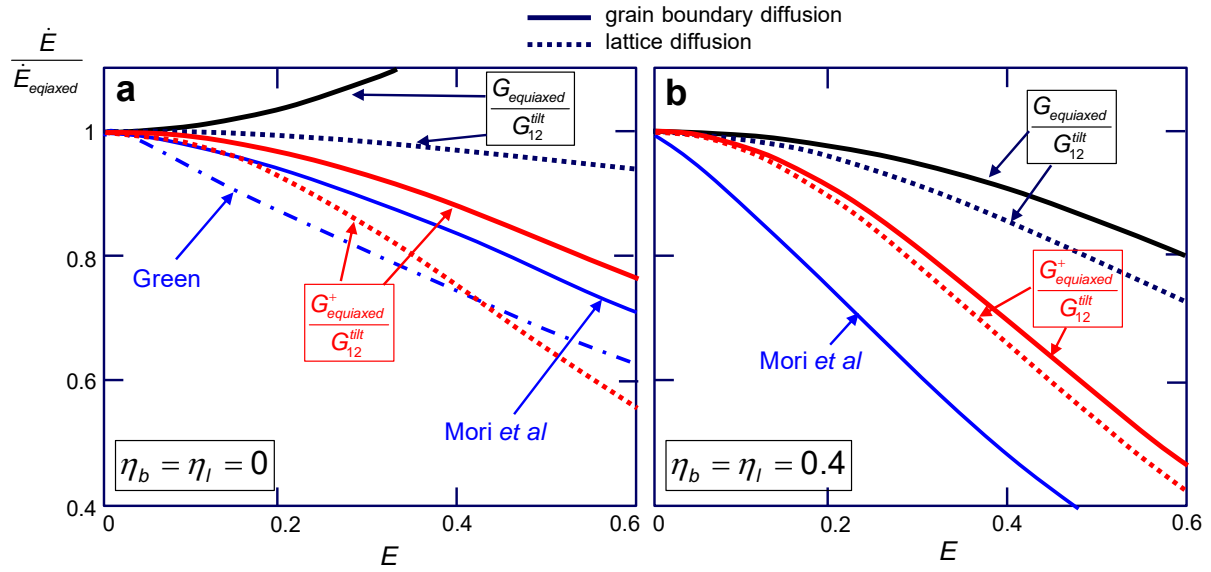


**Figure 7:** Relative evolution of uniaxial creep rate as a function of total strain  $E$  for grain boundary diffusion and lattice diffusion with (a)  $\eta_b = \eta_l = 0$  and (b)  $\eta_b = \eta_l = 0.4$ . Comparison is

made of the ratios  $\frac{G_{eqiaxed}}{G_{tilt_{12}}}$  and  $\frac{G_{eqiaxed}^+}{G_{tilt_{12}}^+}$ , and of the curves derived from Refs (Green, 1970) and (Mori et al., 1998b).

As mentioned in the Introduction, a few authors have already attempted to predict the strain hardening behaviour arising from NHC deformation. The only results that lend themselves to a comparison with present work are due to Green (Green, 1970) and Mori *et al* (Mori et al., 1998b) who, on the basis of the affine hypothesis, modelled the evolution of the uniaxial creep rate of a spherical grain deforming into an ellipsoid. Comparison with present results based on an elliptical grain representation can thus only be qualitative. The curves in blue Fig. 7 have been drawn according to the data reported by these authors. Green (Green, 1970) assumed  $\eta = 0$  and provided a curve valid for both lattice and grain boundary diffusion. Mori *et al* (Mori et al., 1998b) considered only grain boundary diffusion and provided expressions for the dependence of creep rate on  $\eta$ . Globally, the curves derived in the present work on the basis of the effective  $G_{12}^{tilt}$  exhibit a much weaker strain hardening effect than the curves derived from

the data of Green and of Mori et al. The latter curves appear to agree much better with the curves based on of the kinematic bound  $G_{12}^{tilt+}$ . Insofar as the proposed method for estimating the effective  $G_{12}^{tilt}$  is valid, this suggests that the use of pure affine boundary conditions is liable to lead to an overestimation of the strain hardening effect.

The evolution of anisotropy with aspect ratio is highlighted in Figs. 8a and 8b by curves of

variation of the ratio  $\frac{G_{12}^{up}}{G_{12}^{tilt}}$ . Fig.8a presents the dependence of  $\frac{G_{12}^{up}}{G_{12}^{tilt}}$  on  $\eta_b$  or  $\eta_l$  for  $a/b = 2$  (red

curves) and  $a/b = 3$  (blue curves), whereas Fig. 8b presents the dependence on total strain  $E$  for

$\eta_b$  or  $\eta_l = 0.1$  (red curves) and 0.4 (blue curves). The behaviour differs depending on the

diffusion path. In the case of grain boundary diffusion, a large strain-induced anisotropy with

$G_{12b}^{up} > G_{12b}^{tilt}$  is observed when  $\eta$  is small, and the anisotropy decreases when  $\eta$  increases. In

contrast, in the case of lattice diffusion, anisotropy is small when  $\eta$  is small, and an anisotropy

with  $G_{12b}^{up} < G_{12b}^{tilt}$  develops when  $\eta$  increases. It thus appears (i) that grain boundary diffusion

contributes much more to create anisotropy than lattice diffusion (lattice diffusion contributes

to anisotropy only for the statical bound), and (ii) that grain boundary sliding and grain

boundary diffusion have opposite effects on anisotropy. Fig. 8b suggests that, provided the

dominant diffusion mechanism can be identified, it should be possible to access experimentally

the value of  $\eta_b$  or  $\eta_l$  by conducting uniaxial creep tests in two directions on plates or films with

columnar microstructure having sufficiently large transverse to in-plane grain size ratio for

prevalence of plane strain deformation. The creep tests would have to be interrupted at

successive steps of strain amplitude for allowing measurement of both  $\frac{s_{11}^{up}}{s_{11equiaxed}} = \frac{G_{equiaxed}}{G_{12}^{tilt}}$

and  $\frac{s_{11}^{tilt}}{s_{11equiaxed}} = \frac{G_{equiaxed}}{G_{12}^{up}}$  (Eqs. (2), (15) and (16)). The effective value of  $\eta_b$  or  $\eta_l$  would then be

obtained by comparing the experimentally measured evolution of  $\frac{s_{11}^{up}}{s_{11}^{tilt}} = \frac{G_{12}^{up}}{G_{12}^{tilt}}$  with theoretical

curves such as in Fig. 8b.

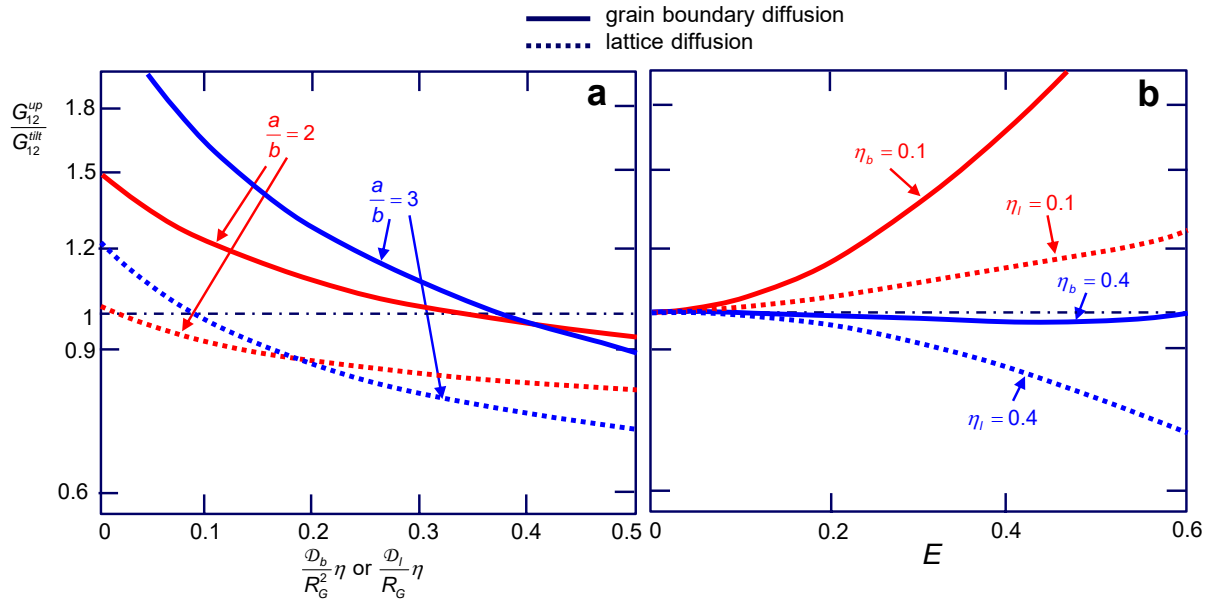


**Figure 8:** Dependence of  $\frac{G_{12}^{up}}{G_{12}^{tilt}}$  (a) on  $\eta_b$  or  $\eta_l$  for  $a/b = 2$  and 3 and (b) on strain  $E$  for  $\eta_b$  or  $\eta_l = 0.1$  and 0.4 (the ordinate scale is logarithmic).

For a polycrystal with randomly isotropic orientation of elongated grains, the effect of grain aspect ratio can be revealed by calculating the average of potentials  $\Psi$  and  $\Phi$  over the orientations  $\alpha$  using the equations provided in the Supplementary Material. It can be verified that this amounts to a Voigt average over the kinematic bounds  $G_{12}^{up+}$  and  $G_{12}^{tilt+}$ , and a Reuss average over the statical bounds  $G_{12}^{up-}$  and  $G_{12}^{tilt-}$ :

$$G_{random}^+ = \frac{1}{2} (G_{12}^{up+} + G_{12}^{tilt+}) \quad (82)$$

$$\text{and } \frac{1}{G_{random}^-} = \frac{1}{2} \left( \frac{1}{G_{12}^{up-}} + \frac{1}{G_{12}^{tilt-}} \right) \quad (83)$$

The curves  $G_{random}^+$  and  $G_{random}^-$  are thus averages of the curves in Figs 3a and 3b, and in Figs 4a and 4b.

## 5. Conclusion

The outcomes of this work can be summarised as follows.

- The two-dimensional viscosity anisotropy ensuing from the alignment of elliptical grains can be characterised by two independent coefficients which can be accessed by considering loading configurations with principal axes oriented at  $0^\circ$  and at  $45^\circ$  with respect to ellipse axes.
- The work illustrates how kinematic (upper) and statical (lower) bounds for the viscosity coefficients can be calculated via power dissipation potentials defined according to variational principles. The kinematic and statical boundary fields can be defined by the affine velocity field and the uniform stress field, respectively. The solutions yielded by these boundary fields may be non-exact.
- The difference between the models proposed in literature for the case of equiaxed grains is elucidated. The general soundness of the affine solution for polycrystals with equiaxed grains is demonstrated.
- For polycrystals with anisotropic grains, a method is proposed for deriving an estimate of the effective viscosity coefficients from the difference between kinematic and statical bounds.

- The work highlights the dependence of viscosity coefficients on boundary viscosity  $\eta$ .  
The increase in grain elongation causes an increase in viscosity, i.e. a strain hardening effect, which increases with  $\eta$ .
- It is suggested that the effective value of  $\eta$  could be characterised experimentally by measuring the evolution of creep strength in two different directions during a creep test.

## Funding

This research did not receive any specific grant from funding agencies in the public, commercial, or not-for-profit sectors.

## Acknowledgements

The authors very gratefully acknowledge the help of John Rudge (Cambridge University UK) in the mathematics, in particular for vectorial calculus with non-orthogonal curvilinear coordinates (Supplementary Material).

## Appendix 1: Assessment of the exactness of trial fields for $\alpha = \frac{\pi}{4}$

The assessment is made only for  $\alpha = \frac{\pi}{4}$  (upright configuration) because it is obvious that, for  $\alpha = 0$  (tilted configuration), it results from symmetry that the resultant moment on the grain is null and the rotation velocity of the grain is null.



### A1.1 Affine velocity field (Eqs. (49) and (50))

If the boundary velocity jump field Eq. (49) and (50) corresponds to an exact solution, the ensuing boundary traction field is equilibrated, i.e. the resultant of forces and moments exerted on the grain vanish (which condition is the global counterpart to the local equilibrium condition  $\nabla \cdot \boldsymbol{\sigma} = 0$ ). If  $\alpha = \frac{\pi}{4}$ , Eqs.(24), (50), and (56) yield

$$T_t = 2\eta_b \frac{R_G^3}{\mathcal{D}_b} \dot{\epsilon} \frac{\cos 2\phi}{A(\phi)} \quad (84)$$

In the case of dominance of grain boundary diffusion, Eqs. (22), (23), and (49) yield

$$T_{bn} = \frac{R_G^3}{\mathcal{D}_b} \dot{\epsilon} c \int_0^\phi A(\phi') \cos 2\phi' d\phi' + T_{bm} \quad (85)$$

The constant term  $T_{bm}$  means the possible existence of a mean stress. It can be verified that the force per unit grain thickness resulting from the boundary traction field Eqs. (84) and (85) is null :

$$\mathbf{F}_b = \begin{pmatrix} \int_S (T_{bn} \sin \beta + T_t \cos \beta) ds \\ \int_S (T_{bn} \cos \beta - T_t \sin \beta) ds \end{pmatrix} = \begin{pmatrix} \int_0^{2\pi} \left( T_{bn} \sqrt{\frac{b}{a}} \cos \phi - T_t \sqrt{\frac{a}{b}} \sin \phi \right) d\phi \\ \int_0^{2\pi} \left( T_{bn} \sqrt{\frac{b}{a}} \cos \phi - T_t \sqrt{\frac{a}{b}} \sin \phi \right) d\phi \end{pmatrix} = 0 \quad (86)$$

The result is different for the moment on the grain,  $\mathbf{M} = \int_S (\mathbf{R} \times \mathbf{T}) ds$ . Prescribing  $\Delta \dot{\epsilon}_t$  by the macroscopic strain rate implies the absence of free rotation of the grain and it follows from Eq. (24) the absence of moment resulting from tangent tractions  $T_t$ . The moment  $M_b$  resulting from the normal traction field (85) is

$$\begin{aligned} M_b &= \int_S T_{bn} R \sin(\beta - \theta) ds \\ &= \frac{e R_G^5}{2 \mathcal{D}_b} \dot{\epsilon} c \int_0^{2\pi} \left[ \int_0^\phi A(\phi') \cos 2\phi' d\phi' \right] \sin 2\phi d\phi \end{aligned} \quad (87)$$

$M_b$  is non-zero, except when  $a=b$ . This shows that Eq. (49) and (50) do not yield an exact

solution for  $\alpha = \frac{\pi}{4}$ , except when  $a=b$ .

In the case of dominance of lattice diffusion, Eqs. (18), (19) and (61) yield, for  $\alpha = \frac{\pi}{4}$ ,

$$T_{ln} = \frac{1}{2} \frac{kTR_G^2}{\Omega D_l} \dot{E} c \frac{\sin 2\phi}{A(\phi)} + T_{lm} \quad (88)$$

Again, the constant term  $T_{lm}$  means the possible existence of a mean stress. Via Eq. (86), it can be verified that the resultant force per unit grain thickness arising from boundary tractions is null. Conversely, the moment  $M_l$  resulting from the normal traction field (88) is

$$\begin{aligned} M_l &= \int_S T_{nl} R \sin(\beta - \theta) ds \\ &= -\frac{e}{4} \frac{kTR_G^4}{\Omega D_l} \dot{E} c \int_0^{2\pi} \frac{\sin^2 2\phi}{A(\phi)} d\phi \end{aligned} \quad (89)$$

$M_l$  does not vanish, except when  $a=b$ . The non-exactness of the two solutions results from the choice of a kinematic boundary field that does not involve grain rotation (Wheeler, 2010).

#### A1.2 Uniform stress field (Eqs. (67) and (68))

In this case, the existence of grain translation and/or rotation does not mean that the trial boundary traction field does not yield an exact solution: the only criterion for the exactness of the solution is that the corresponding boundary velocity field involve no change of grain volume. It follows from Eq. (24) that, if  $T_t$  is prescribed by the macroscopic stress (Eq. (68)), the tangent velocity jump field  $\Delta \dot{U}_t$  involves neither a change of grain volume, nor a translation or rotation of the grain. A volume change or a translation/rotation of the grain can thus arise only from the normal velocity jump field  $\Delta \dot{U}_n$ . As detailed in the Supplementary Material, the

coupling of Eqs. (22), (23), and (67) yields, if  $\alpha = \frac{\pi}{4}$ ,

$$\Delta \dot{u}_{bn} = 4 \frac{\mathcal{D}_b}{R_G^2} S \frac{\sin 2\phi}{A^6(\phi)} \left[ \frac{a}{b} + \frac{e}{4} \left( \frac{a \cos 2\phi}{b A^6(\phi)} - 2 - e \frac{1}{A^6(\phi)} \right) \right] \quad (90)$$

The change of volume due to  $\Delta \dot{u}_{bn}$  writes

$$\begin{aligned} \langle \dot{\epsilon}_{11} \rangle + \langle \dot{\epsilon}_{22} \rangle &= \frac{1}{2V} \int_S \Delta \dot{u}_{bn} ds \\ &= \frac{\mathcal{D}_b}{R_G^3} S \frac{2}{\pi} \left\{ \int_0^{2\pi} \frac{\sin 2\phi}{A^6(\phi)} \left[ \frac{a}{b} + \frac{e}{4} \left( \frac{a \cos 2\phi}{b A^6(\phi)} - 2 - e \frac{1}{A^6(\phi)} \right) \right] d\phi \right\}, \end{aligned} \quad (91)$$

the translation velocity of the grain writes

$$\begin{aligned} \dot{\mathbf{u}}_O - \dot{\mathbf{u}}_{surroundings} &= \frac{1}{S} \int_S (\Delta \dot{u}_{nb} \sin \beta \mathbf{x}_1 + \Delta \dot{u}_{nb} \cos \beta \mathbf{x}_2) ds \\ &= \frac{1}{2\pi} \int_S \left( \Delta \dot{u}_{nb} \sqrt{\frac{a}{b}} \sin \phi \mathbf{x}_1 + \Delta \dot{u}_{nb} \sqrt{\frac{b}{a}} \cos \phi \mathbf{x}_2 \right) d\phi, \end{aligned} \quad (92)$$

and the rotation velocity of the grain with respect to its neighbours writes

$$\begin{aligned} \dot{\theta}_b &= \frac{1}{S} \int_S \frac{\Delta \dot{u}_{nb}}{2} \frac{1}{R} \sin(\beta - \theta) ds \\ &= e \frac{1}{\pi} \frac{\mathcal{D}_b}{R_G^4} S \int_0^{2\pi} \frac{\sin^2 2\phi}{A^7(\phi) B(\phi)} \left[ \frac{a}{b} + \frac{e}{4} \left( \frac{a \cos 2\phi}{b A^6(\phi)} - 2 - e \frac{1}{A^6(\phi)} \right) \right] d\phi \end{aligned} \quad (93)$$

It can be verified that all integrals of the terms in Eqs (91) and (92) are zero, which means the absence of volume change and of translation of the grain. In contrast, it follows from Eq. (93) that, unless  $a = b$ ,  $\dot{\theta}_b$  is non-null: mechanical equilibrium requires a certain rotation velocity of the grain.

In the case of dominance of lattice diffusion, Eqs. (18) and (23) yield, if  $\alpha = \frac{\pi}{4}$

$$\Delta \dot{u}_{ln} = 4 \frac{\Omega D_l}{kT} \frac{1}{R_G} S \frac{\sin 2\phi}{A(\phi)} \quad (94)$$

In the same way as above, it can be verified that this velocity jump field implies not only the conservation of volume and the absence of grain translation, but also a rotation velocity  $\dot{\theta}_l \neq 0$ , unless  $a = b$ . This rotation velocity is required for mechanical equilibrium.

## Appendix 2 : Exact solutions for equiaxed grains

As shown in Appendix 1, when  $a = b$ , the two solutions brought about by trial fields Eqs (27) and (28) are distinct exact solutions in the sense that they both respect mechanical equilibrium, conservation of mass, and continuity of diffusion potential. In Ref. Brassart and Delannay, (2019), a similar couple of solutions arising from kinematic and statical boundary conditions was identified in the framework of a 3D-model based on a spherical grain. The existence of two distinct solutions is justified by the statistical nature of the model, which does not involve a RVE suitable to fill the space and a simplified description of the mechanical interactions between neighbouring grains. The question then arises of whether other exact solutions can exist for such a statistical model. In this Appendix, we address this question by assessing the possible existence of other trial fields respecting Hill's lemma, i.e. the equality of macroscopic power and average microscopic power expended in the grain. We consider only the case  $a = b$  with dominance of grain boundary diffusion.

Only the orientation  $\alpha = 0$  needs to be considered. The symmetry of the problem implies that, with respect to  $\theta$ , the solutions are periodic with period  $\pi/2$ . This imposes that velocity and traction fields be expressible under the form of Fourier series:

$$\Delta \dot{u}_n = 2R_G \dot{E} \sum_{m=1}^{\infty} A_m \cos 2m\theta \quad (95)$$

$$\Delta \dot{\epsilon}_t = -2R_G \dot{\epsilon} \sum_{m=1}^{\infty} B_m \sin 2m\theta \quad (96)$$

$$T_n = S \sum_{m=1}^{\infty} A'_m \cos 2m\theta \quad (97)$$

$$T_t = -S \sum_{m=1}^{\infty} B'_m \sin 2m\theta \quad (98)$$

where  $A_m$ ,  $B_m$ ,  $A'_m$ , and  $B'_m$  are non-dimensional factors. It follows from Eq. (53)

$$j_b = -R_G^2 \dot{\epsilon} \sum_{m=1}^{\infty} \frac{1}{m} A_m \sin 2m\theta \quad (99)$$

whereas it follows from Eq. (85)

$$T_n = \frac{1}{2} \dot{\epsilon} \frac{R_G^3}{\mathcal{D}_b} \sum_{m=1}^{\infty} \frac{1}{m^2} A_m \cos 2m\theta \quad (100)$$

Eqs (97) and (100) bring

$$\frac{A'_m}{A_m} = \frac{1}{2m^2} \frac{\dot{\epsilon} R_G^3}{S \mathcal{D}_b} \quad (101)$$

Similarly, Eq. (24) brings

$$\frac{B'_m}{B_m} = 2\eta R_G \frac{\dot{\epsilon}}{S} = 2\eta_b \frac{\dot{\epsilon} R_G^3}{S \mathcal{D}_b} \quad (102)$$

Via Eqs (25), (26), (95), and (98), we can derive the volume averages of strain rate tensor and stress tensor:

$$\begin{aligned} \langle \dot{\epsilon}_{xx} \rangle &= \frac{1}{2V} \int_S 2 \left( n_x \frac{\Delta \dot{\epsilon}_x}{2} \right) dS \\ &= \dot{\epsilon} \frac{1}{\pi} \int_0^{2\pi} \left( \sin^2 \theta \sum_{m=1}^{\infty} A_m \cos 2m\theta - \frac{1}{2} \sin 2\theta \sum_{m=1}^{\infty} B_m \sin 2m\theta \right) d\theta \\ &= -\frac{1}{2} \dot{\epsilon} (A_1 + B_1) \end{aligned} \quad (103)$$

$$\langle \dot{\epsilon}_{zz} \rangle = \frac{1}{2V} \int_S 2 \left( n_z \frac{\Delta \dot{u}_z}{2} \right) dS = \frac{1}{2} \dot{E} (A_1 + B_1) \quad (104)$$

$$\langle \dot{\epsilon}_{xz} \rangle = \frac{1}{2V} \int_S \left( n_x \frac{\Delta \dot{u}_z}{2} + n_z \frac{\Delta \dot{u}_x}{2} \right) dS = 0 \quad (105)$$

$$\begin{aligned} \langle \sigma_{zz} \rangle &= -\langle \sigma_{xx} \rangle = \frac{1}{2} S (A'_1 + B'_1) \\ &= \frac{1}{2} \dot{E} \left( \frac{1}{2} A_1 + 2\eta_b B_1 \right) \frac{R_G^3}{\mathcal{D}_b} \end{aligned} \quad (106)$$

$$\langle \sigma_{xz} \rangle = 0 \quad (107)$$

It follows from conditions  $\langle \dot{\epsilon}_{ij} \rangle \equiv \dot{E}_{ij}$  and  $\langle \sigma_{ij} \rangle \equiv S_{ij}$  together with Eqs (104) and (106)

$$\frac{1}{2} (A_1 + B_1) = 1 \quad (108)$$

$$\text{and} \quad \frac{1}{2} (A'_1 + B'_1) = 1 \quad (109)$$

Via Parseval identity, Eq. (99) yields the dissipation due to grain boundary diffusion as

$$\begin{aligned} \dot{Q}_b &= \frac{1}{\pi R_G^2} \frac{1}{2} \frac{R_G}{\mathcal{D}_b} \int_0^{2\pi} \left( -R_G^2 \dot{E} \sum_{m=1}^{\infty} \frac{1}{m} A_m \sin 2m\theta \right)^2 d\theta \\ &= \frac{1}{2} \dot{E}^2 \frac{R_G^3}{\mathcal{D}_b} \sum_{m=1}^{\infty} \left( \frac{A_m}{m} \right)^2 \end{aligned} \quad (110)$$

Similarly, the dissipation due to grain boundary sliding is obtained from Eq. (96) as

$$\dot{Q}_{sl} = 2\eta_b \dot{E}^2 \frac{R_G^3}{\mathcal{D}_b} \sum_{m=1}^{\infty} (B_m)^2 \quad (111)$$

Equality of work power and dissipation rate writes

$$\dot{Q}_b + \dot{Q}_{sl} = 2 \langle \dot{\epsilon}_{zz} \rangle \langle \sigma_{zz} \rangle \quad (112)$$

which develops into

$$\frac{1}{2} \sum_{n=1}^{\infty} \left( \frac{A_n}{m} \right)^2 + 2\eta_b \sum_{m=1}^{\infty} (B_m)^2 = \frac{1}{2} \left( \frac{1}{2} A_1^2 + \left( \frac{1}{2} + 2\eta_b \right) A_1 B_1 + 2\eta_b B_1^2 \right) \quad (113)$$

This means that an exact solution requires  $A_m = B_m = 0$  for all  $m > 1$ . One ends up with the second-degree equation

$$\frac{A_1^2}{B_1^2} - (1 + 4\eta_b) \frac{A_1}{B_1} + 4\eta_b = 0. \quad (114)$$

This equation admits two solutions:

- a)  $\frac{A_1}{B_1} = 1$  i.e., from Eq. (108),  $A_1 = B_1 = 1$ , which is the solution obtained using a trial field assuming prescribed velocities;
- b)  $\frac{A_1}{B_1} = 4\eta_b$ , i.e., from Eqs (106) and (109),  $A'_1 = B'_1 = 1$ , which is the solution obtained using a trial field assuming prescribed tractions.

This demonstration shows that, if  $a = b$ , there exists no other trial field able to satisfy Hill's lemma. It also shows that the two solutions coincide when  $\eta_b = \frac{1}{4}$ . It can be shown that, in the latter case, the mean stress is uniformly null inside the volume of the grain.

## References

- Ashby, M., Verrall, R., 1973. Diffusion-accommodated flow and superplasticity. *Acta Metallurgica* 21, 149-163.
- Balluffi, R.W., Allen, S., Carter, W.C., 2005. *Kinetics of materials*. John Wiley & Sons.
- Beere, W., 1977. Grain-boundary sliding controlled creep: its relevance to grain rolling and superplasticity. *Journal of Materials Science* 12, 2093-2098.
- Brassart, L., Delannay, F., 2019. Bounds for shear viscosity in Nabarro–Herring–Coble creep. *Mech Mater* 137, 103106.
- Burton, B., 1994. Anisotropy of grain-boundary diffusional creep in a polycrystalline array with orthorhombic grain geometry. *Philosophical Magazine A* 69, 565-582.
- Burton, B., Greenwood, G., 1985. Analysis of Coble creep in cylindrical and cubic crystals. *Mater. Sci. Technol.* 1, 1029-1032.
- Cannon, W.R., 1972. The contribution of grain boundary sliding to axial strain during diffusion creep. *Philosophical Magazine* 25, 1489-1497.
- Coble, R., 1963. A model for boundary diffusion controlled creep in polycrystalline materials. *J Appl Phys* 34, 1679-1682.
- Cocks, A., 1996. Variational principles, numerical schemes and bounding theorems for deformation by Nabarro-Herring creep. *Journal of the Mechanics and Physics of Solids* 44, 1429-1452.
- Destrade, M., Martin, P.A., Ting, T.C., 2002. The incompressible limit in linear anisotropic elasticity, with applications to surface waves and elastostatics. *Journal of the Mechanics and Physics of Solids* 50, 1453-1468.
- Green, H., 1970. Diffusional flow in polycrystalline materials. *J Appl Phys* 41, 3899-3902.
- Greenwood, G.W., 1992. A formulation for anisotropy in diffusional creep. *Proc. R. Soc. Lond. A* 436, 187-196.
- Hearmon, R.F.S., 1961. *An introduction to applied anisotropic elasticity*. Oxford University Press.
- Herring, C., 1950. Diffusional Viscosity of a Polycrystalline Solid. *J Appl Phys* 21, 437-445.
- Itskov, M., Aksel, N., 2002. Elastic constants and their admissible values for incompressible and slightly compressible anisotropic materials. *Acta Mechanica* 157, 81-96.
- Kim, B.-N., Hiraga, K., Morita, K., Ahn, B.-W., 2004. Analysis of creep due to grain-boundary diffusion in hexagonal microstructures. *Philosophical Magazine* 84, 3251-3262.
- Kim, B.-N., Hiraga, K., Morita, K., Yoshida, H., Ahn, B.-W., 2009. Viscous grain-boundary sliding with rotating particles or grains. *Acta Materialia* 57, 5730-5738.
- Kim, B.-N., Morita, K., Hiraga, K., 2003. Rate of diffusion creep accompanied by grain boundary sliding in elongated microstructures. *Materials Science and Engineering: A* 363, 67-71.
- Lee, D., 1970. Structural changes during the superplastic deformation. *Metallurgical and Materials Transactions B* 1, 309-311.
- Li, Y., Li, S., Huang, M., Li, Z., 2015. Analytical solution for Coble creep in polycrystalline materials under biaxial loading. *Mech Mater* 91, 290-294.
- Lifshitz, I., 1963. On the theory of diffusion-viscous flow of polycrystalline bodies. *Soviet Physics JETP* 17, 909-920.
- McMeeking, R., Kuhn, L., 1992. A diffusional creep law for powder compacts. *Acta metallurgica et materialia* 40, 961-969.



- Mori, T., Nakasone, Y., Taya, M., Wakashima, K., 1997. Steady-state creep rate of a composite: Two-dimensional analysis. *Philosophical Magazine Letters* 75, 359-365.
- Mori, T., Onaka, S., Wakashima, K., 1998a. Role of grain-boundary sliding in diffusional creep of polycrystals. *J Appl Phys* 83, 7547-7552.
- Mori, T., Taya, M., Wakashima, K., 1998b. Steady-state creep of a composite analysed by an energy balance method. *Philosophical Magazine Letters* 78, 331-338.
- Nabarro, F.R.N., 1948. Deformation of crystals by the motion of single ions, Conference on Strength of Solids. Physical Society London, Bristol, pp. 75-90.
- Nye, J.F., 1957. *Physical Properties of Crystals*. Oxford Science Publications.
- Onaka, S., Huang, J., Wakashima, K., Mori, T., 1998. Kinetics of stress relaxation caused by the combination of interfacial sliding and diffusion: two-dimensional analysis. *Acta Materialia* 46, 3821-3828.
- Onaka, S., Madgwick, A., Mori, T., 2001. Kinetics of diffusional creep discussed by energy dissipation and effect of grain-size distribution on the rate equations. *Acta Materialia* 49, 2161-2168.
- Pan, J., Cocks, A.C.F., 1993. Computer simulation of superplastic deformation. *Comput Mater Sci* 1, 95-109.
- Ponte-Castañeda, P., Willis, J.R., 1995. The effect of spatial distribution on the effective behavior of composite materials and cracked media. *Journal of the Mechanics and Physics of Solids* 43, 1919-1951.
- Rachinger, W.A., 1952. *J. Inst. Metals* 81, 33.
- Raj, R., Ashby, M., 1971. On grain boundary sliding and diffusional creep. *Metallurgical transactions* 2, 1113-1127.
- Reddy, J.N., 2013. *An Introduction to Continuum Mechanics* 2nd Ed. Cambridge University Press.
- Rudge, J.F., 2018. The Viscosities of Partially Molten Materials Undergoing Diffusion Creep. *Journal of Geophysical Research: Solid Earth* 123, 10,534-510,562.
- Spingarn, J., Nix, W., 1978. Diffusional creep and diffusionally accommodated grain rearrangement. *Acta Metallurgica* 26, 1389-1398.
- Takei, Y., Holtzman, B.K., 2009. Viscous constitutive relations of solid-liquid composites in terms of grain boundary contiguity: 1. Grain boundary diffusion control model. *Journal of Geophysical Research: Solid Earth* 114.
- Wei, Y., Bower, A.F., Gao, H., 2008. Recoverable creep deformation and transient local stress concentration due to heterogeneous grain-boundary diffusion and sliding in polycrystalline solids. *Journal of the Mechanics and Physics of Solids* 56, 1460-1483.
- Wheeler, J., 2009. The preservation of seismic anisotropy in the Earth's mantle during diffusion creep. *Geophysical Journal International* 178, 1723-1732.
- Wheeler, J., 2010. Anisotropic rheology during grain boundary diffusion creep and its relation to grain rotation, grain boundary sliding and superplasticity. *Philosophical Magazine* 90, 2841-2864.

## Figure Captions

Figure 1: Statistical model representing grains as elliptical cylinders with principal axes oriented in the same direction. Angle  $\alpha$  represents a rotation of the coordinate system around axis 3.

Figure 2: Definition of coordinate systems

Figure 3: Grain boundary diffusion: dependence on boundary viscosity coefficient  $\eta$  of the upper and lower bounds for (a)  $G_{12b}^{up}$  and (b)  $G_{12b}^{tilt}$  for  $a/b = 1, 2$ , and  $3$ .

Figure 4: Lattice diffusion: dependence on  $\eta$  of the upper and lower bounds for (a)  $G_{12l}^{up}$  and (b)  $G_{12l}^{tilt}$  for  $a/b = 1, 2$ , and  $3$ .

Figure 5: Dependence on  $\eta$  of the kinematic and statical solutions,  $G_{equiaxed}^+$  (continuous black) and  $G_{equiaxed}^-$  (dashed black), for the two diffusion modes (Eqs. (59), (66), (71), and (75)) together with the kinematic solutions for a hexagonal lattice of grains,  $G_{b_{hexag.}}$  (red) and  $G_{l_{hexag.}}$  (blue) (Eqs. (78) and (79)), and the statical solution for a hexagonal grain,  $G_{b_{hexag.}}^-$  (Eq. (80)).

Figure 6: Comparison of the curve  $G_{b_{hexag.}}$  drawn according to Eq. (78) with FEM simulations of a random 2D polycrystal (Wei et al., 2008)

Figure 7: Relative evolution of uniaxial creep rate as a function of total strain  $E$  for grain boundary diffusion and lattice diffusion with (a)  $\eta_b = \eta_l = 0$  and (b)  $\eta_b = \eta_l = 0.4$ . Comparison is made of the ratios  $\frac{G_{equiaxed}}{G_{12}^{tilt}}$  and  $\frac{G_{equiaxed}}{G_{12}^{tilt+}}$  and of the curves derived from Refs (Green, 1970) and (Mori et al., 1998b).

Figure 8: Dependence of  $\frac{G_{12}^{up}}{G_{12}^{tilt}}$  (a) on  $\eta_b$  or  $\eta_l$  for  $a/b = 2$  and 3 and (b) on strain  $E$  for  $\eta_b$  or  $\eta_l = 0.1$  and 0.4 (the ordinate scale is logarithmic).

**Table 1** : list of symbols*Material properties and physical constants*

$k$	Boltzmann's constant (energy per atom and per Kelvin)
$D_b$	grain boundary diffusion coefficient (area per unit time)
$D_l$	lattice diffusion coefficient (area per unit time)
$\eta$	boundary viscosity coefficient at grain boundary (force * time per unit volume)
$\eta_b$	boundary viscosity coefficient defined in Eq. (56) (non-dimensional)
$\eta_l$	boundary viscosity coefficient defined in Eq. (63) (non-dimensional)
$\Omega$	volume per atom

*Scalars and scalar functions*

$a$	half major axis of ellipse
$b$	half minor axis of ellipse
$c$	geometrical parameter defined in Eq. (56) (non-dimensional)
$e$	geometrical parameter defined in Eq. (41) (non-dimensional)
$s$	curvilinear coordinate along ellipse boundary
$A(\phi)$	function of $\phi$ defined in Eq. (42) (non-dimensional)
$B(\phi)$	function of $\phi$ defined in Eq. (38) (non-dimensional)
$E$	total accumulated strain along principal tensile direction
$\dot{E}$	macroscopic strain rate along principal tensile direction
$F_b(\alpha)$	integration constant defined in Eq. (55) (non-dimensional)
$G$	isotropic shear viscosity (force * time per unit surface)
$R_G$	radius of circular cylinder with same cross sectional area as grain average
$S$	macroscopic stress along principal tensile direction
$V$	grain volume
$\alpha$	rotation of coordinate system axes with respect ellipse axes
$\beta$	orientation of normal vector $\mathbf{n}$ with respect to coordinate axis 2 (Fig. 2)
$\gamma$	parameter defined in Eq. (74) (non-dimensional)
$\delta$	thickness of grain boundary layer

$\phi$	azimuthal coordinate defined in Fig. 2
$\lambda(\alpha)$	function defined in Eqs. (62) (non-dimensional)
$\mu$	diffusion potential (energy per atom)
$\theta$	azimuthal angle defined with respect to coordinate axis 2 (Fig. 2)
$\dot{\theta}$	grain rotation velocity
$\rho$	radial coordinate defined in Fig. 2
$\Phi$	dissipation potential defined by Eq. (33) (energy per unit time per unit volume)
$\Psi$	dissipation potential defined by Eq. (30) (energy per unit time per unit volume)

*Vectors, tensors, and matrices*

<b>c</b>	viscous stiffness matrix (force * time per unit surface)
<b>n</b>	unit vector normal to ellipse
$j_b$	grain boundary diffusion flux (volume per unit length per unit time)
<b>s</b>	viscous compliance matrix (surface per unit force per unit time)
<b>t</b>	unit vector tangent to ellipse
$\dot{\mathbf{u}}$	local velocity vector
<b>x</b>	position vector
$\dot{\mathbf{E}}$	macroscopic strain rate tensor
<b>F</b>	force on the grain per unit grain thickness
<b>M</b>	moment on the grain per unit grain thickness
<b>R</b>	vector connecting grain centroid to grain boundary
$J_l$	lattice diffusion flux (volume per unit surface per unit time)
<b>S</b>	macroscopic stress tensor
<b>T</b>	traction vector on ellipse boundary
$\dot{\boldsymbol{\varepsilon}}$	local strain rate tensor
$\boldsymbol{\sigma}$	local stress tensor
$\Delta \dot{\mathbf{u}}$	velocity jump vector at ellipse boundary

## Supplementary Material

### *Details of mathematical developments in paper*

#### Variational analysis of the influence of grain shape anisotropy on shear viscosity

##### in Nabarro-Herring-Coble creep

Francis Delannay and Laurence Brassart

## 2. Principles

### 2.4. Transformation of coordinates

Eq. (40) can be developed as follows

$$\begin{aligned}
 R &= R_G B(\phi) = \sqrt{ab} B(\phi) \\
 X_2 &= R \cos \theta = a \cos \phi \\
 \cos \theta &= \frac{a}{R} \cos \phi = \frac{1}{\sqrt{\frac{b}{a} + e \cos^2 \phi}} \sqrt{\frac{a}{b}} \cos \phi \\
 \cos \theta d\theta &= \frac{\cos \phi}{\frac{b}{a} + e \cos^2 \phi} \left( \sqrt{\frac{b}{a}} \sqrt{\frac{b}{a} + e \cos^2 \phi} + e \frac{\sqrt{\frac{b}{a}} \sin \phi \sin \phi}{\sqrt{\frac{b}{a} + e \cos^2 \phi}} \right) d\phi \\
 \frac{1}{\sqrt{\frac{b}{a} + e \cos^2 \phi}} \sqrt{\frac{a}{b}} \cos \phi d\theta &= \sqrt{\frac{b}{a}} \frac{\cos \phi}{\frac{b}{a} + e \cos^2 \phi} \left( \sqrt{\frac{b}{a} + e \cos^2 \phi} + e \frac{\sin^2 \phi}{\sqrt{\frac{b}{a} + e \cos^2 \phi}} \right) d\phi \\
 d\theta &= \frac{b}{a} \frac{1}{\frac{b}{a} + e \cos^2 \phi} \left( \left( \frac{b}{a} + e \cos^2 \phi \right) + e \sin^2 \phi \right) d\phi \\
 d\theta &= \frac{\frac{b}{a} \left( \frac{b}{a} + e \right)}{\frac{b}{a} + e \cos^2 \phi} d\phi = \frac{1}{\frac{b}{a} + e \cos^2 \phi} d\phi
 \end{aligned} \tag{A.1}$$

This yields

$$d\theta = \frac{1}{B^2(\phi)} d\phi \quad (\text{A.2})$$

Eq. (45) can be developed as follows:

$$\begin{aligned} \tan \theta &= \frac{b}{a} \tan \phi \\ \tan \beta &= \frac{a}{b} \tan \phi \\ \cos(\beta - \theta) &= \sin \theta \sin \beta + \cos \theta \cos \beta \\ &= \frac{1}{\sqrt{1 + \left(\frac{b}{a} \tan \phi\right)^{-2}}} \frac{1}{\sqrt{1 + \left(\frac{a}{b} \tan \phi\right)^{-2}}} + \frac{1}{\sqrt{1 + \left(\frac{b}{a} \tan \phi\right)^2}} \frac{1}{\sqrt{1 + \left(\frac{a}{b} \tan \phi\right)^2}} \\ &= \frac{1}{\sqrt{1 + \left(\frac{b^2}{a^2} + \frac{a^2}{b^2}\right) \tan^2 \phi + \tan^4 \phi}} + \frac{1}{\sqrt{1 + \left(\frac{b^2}{a^2} + \frac{a^2}{b^2}\right) \tan^2 \phi + \tan^4 \phi}} \\ &= \frac{1}{\sqrt{1 + \left(\frac{b^2}{a^2} + \frac{a^2}{b^2}\right) \tan^2 \phi + \tan^4 \phi}} (1 + \tan^2 \phi) \\ &= \frac{1}{\cos^2 \phi} \frac{1}{\sqrt{1 + \left(\frac{b^2}{a^2} + \frac{a^2}{b^2}\right) \tan^2 \phi + \tan^4 \phi}} \\ &= \frac{1}{\sqrt{\cos^4 \phi + \left(\frac{b^2}{a^2} + \frac{a^2}{b^2}\right) \sin^2 \phi \cos^2 \phi + \sin^4 \phi}} \\ &= \frac{1}{\sqrt{1 + \left(\frac{b^2}{a^2} + \frac{a^2}{b^2} - 2\right) \sin^2 \phi \cos^2 \phi}} \\ &= \frac{1}{\sqrt{1 + \left(\frac{e}{2}\right)^2 \sin^2 2\phi}} = \frac{1}{\sqrt{\frac{a}{b} - e \cos^2 \phi} \sqrt{\frac{b}{a} + e \cos^2 \phi}} \end{aligned} \quad (\text{A.3})$$

This yields

$$\mathbf{n} \cdot \mathbf{R} = R \cos(\beta - \theta) = \frac{R}{A(\phi)B(\phi)} \quad (\text{A.4})$$

### 3. Results

#### 3.1 Kinematic boundary conditions based on an affine velocity field

Eq. (49) is obtained as follows:

$$\begin{aligned}
 \Delta \dot{u}_n &= \Delta \dot{\mathbf{u}} \cdot \mathbf{n} \\
 &= 2R\dot{E} \left[ \cos 2\alpha (\cos \beta \cos \theta - \sin \beta \sin \theta) + \sin 2\alpha (\cos \theta \sin \beta + \sin \theta \cos \beta) \right] \quad (\text{A.5}) \\
 &= 2R\dot{E} \left[ \cos 2\alpha \cos(\theta + \beta) + \sin 2\alpha \sin(\theta + \beta) \right]
 \end{aligned}$$

$$\begin{aligned}
 \cos(\theta + \beta) &= -\sin \theta \sin \beta + \cos \theta \cos \beta \\
 &= -\frac{1}{\sqrt{1 + \left(\frac{b}{a} \tan \phi\right)^2}} \frac{1}{\sqrt{1 + \left(\frac{a}{b} \tan \phi\right)^2}} + \frac{1}{\sqrt{1 + \left(\frac{b}{a} \tan \phi\right)^2}} \frac{1}{\sqrt{1 + \left(\frac{a}{b} \tan \phi\right)^2}} \\
 &= -\frac{1}{\sqrt{1 + \left(\frac{b^2}{a^2} + \frac{a^2}{b^2}\right) \tan^2 \phi + \tan^4 \phi}} + \frac{1}{\sqrt{1 + \left(\frac{b^2}{a^2} + \frac{a^2}{b^2}\right) \tan^2 \phi + \tan^4 \phi}} \\
 &= \frac{1}{\sqrt{1 + \left(\frac{b^2}{a^2} + \frac{a^2}{b^2}\right) \tan^2 \phi + \tan^4 \phi}} (1 - \tan^2 \phi) \\
 &= \frac{\cos 2\phi}{\cos^2 \phi} \frac{1}{\sqrt{1 + \left(\frac{b^2}{a^2} + \frac{a^2}{b^2}\right) \tan^2 \phi + \tan^4 \phi}} \\
 &= \frac{\cos 2\phi}{\sqrt{\cos^4 \phi + \left(\frac{b^2}{a^2} + \frac{a^2}{b^2}\right) \sin^2 \phi \cos^2 \phi + \sin^4 \phi}} \\
 &= \frac{\cos 2\phi}{\sqrt{1 + \left(\frac{b^2}{a^2} + \frac{a^2}{b^2} - 2\right) \sin^2 \phi \cos^2 \phi}} \\
 &= \frac{\cos 2\phi}{\sqrt{1 + \left(\frac{e}{2}\right)^2 \sin^2 2\phi}}
 \end{aligned} \tag{A.6}$$



$$\begin{aligned}
\sin(\theta + \beta) &= \cos \theta \sin \beta + \sin \theta \cos \beta \\
&= \frac{1}{\sqrt{1 + \left(\frac{b}{a} \tan \phi\right)^2}} \frac{1}{\sqrt{1 + \left(\frac{a}{b} \tan \phi\right)^{-2}}} + \frac{1}{\sqrt{1 + \left(\frac{b}{a} \tan \phi\right)^{-2}}} \frac{1}{\sqrt{1 + \left(\frac{a}{b} \tan \phi\right)^2}} \\
&= \frac{1}{\sqrt{1 + \left(\frac{b}{a}\right)^4 + \left(\frac{a}{b} \tan \phi\right)^{-2} + \left(\frac{b}{a} \tan \phi\right)^2}} + \frac{1}{\sqrt{1 + \left(\frac{a}{b}\right)^4 + \left(\frac{b}{a} \tan \phi\right)^{-2} + \left(\frac{a}{b} \tan \phi\right)^2}} \\
&= \frac{1}{\sqrt{1 + \left(\frac{b}{a}\right)^4 + \left(\frac{a}{b} \tan \phi\right)^{-2} + \left(\frac{b}{a} \tan \phi\right)^2}} \left(1 + \frac{b^2}{a^2}\right) \\
&= \frac{1}{\sqrt{\left(1 + \left(\frac{b}{a}\right)^4\right) \left(\frac{a}{b} \tan \phi\right)^2 + 1 + \left(\frac{b}{a} \tan \phi\right)^2 \left(\frac{a}{b} \tan \phi\right)^2}} \left(1 + \frac{b^2}{a^2}\right) \frac{a}{b} \tan \phi \\
&= \frac{1}{\sqrt{1 + \left(\frac{b^2}{a^2} + \frac{a^2}{b^2}\right) \tan^2 \phi + \tan^4 \phi}} \left(\frac{a}{b} + \frac{b}{a}\right) \tan \phi \\
&= \frac{1}{2} \left(e + 2 \frac{b}{a}\right) \sin 2\phi \frac{1}{\sqrt{\cos^4 \phi + \left(\frac{b^2}{a^2} + \frac{a^2}{b^2}\right) \sin^2 \phi \cos^2 \phi + \sin^4 \phi}} \\
&= \left(\frac{e}{2} + \frac{b}{a}\right) \sin 2\phi \frac{1}{\sqrt{1 + \left(\frac{e}{2}\right)^2 \sin^2 2\phi}}
\end{aligned} \tag{A.7}$$

$$\begin{aligned}
\Delta \dot{u}_n &= 2R\dot{E} \left[ \cos 2\alpha \cos(\theta + \beta) + \sin 2\alpha \sin(\theta + \beta) \right] \\
&= 2R\dot{E} \left[ \cos 2\alpha \frac{\cos 2\phi}{\sqrt{1 + \left(\frac{e}{2}\right)^2 \sin^2 2\phi}} + \sin 2\alpha \left(\frac{e}{2} + \frac{b}{a}\right) \sin 2\phi \frac{1}{\sqrt{1 + \left(\frac{e}{2}\right)^2 \sin^2 2\phi}} \right] \\
&= 2R_G \dot{E} \frac{\sqrt{\frac{b}{a} + e \cos^2 \phi}}{\sqrt{1 + \left(\frac{e}{2}\right)^2 \sin^2 2\phi}} \left( \cos 2\alpha \cos 2\phi + \left(\frac{e}{2} + \frac{b}{a}\right) \sin 2\alpha \sin 2\phi \right) \\
&= 2R_G \dot{E} \frac{1}{\sqrt{\frac{a}{b} - e \cos^2 \phi}} \frac{\sqrt{\frac{a}{b} - e \cos^2 \phi} \sqrt{\frac{b}{a} + e \cos^2 \phi}}{\sqrt{1 + \left(\frac{e}{2}\right)^2 \sin^2 2\phi}} \left( \cos 2\alpha \cos 2\phi + \left(\frac{e}{2} + \frac{b}{a}\right) \sin 2\alpha \sin 2\phi \right) \\
&= 2R_G \dot{E} \frac{1}{\sqrt{\frac{a}{b} - e \cos^2 \phi}} \sqrt{\frac{1 + \frac{a}{b} e \cos^2 \phi - \frac{b}{a} e \cos^2 \phi - e^2 \cos^4 \phi}{1 + \frac{1}{4} e^2 \sin^2 2\phi}} \left( \cos 2\alpha \cos 2\phi + \left(\frac{e}{2} + \frac{b}{a}\right) \sin 2\alpha \sin 2\phi \right) \\
&= 2R_G \dot{E} \frac{1}{\sqrt{\frac{a}{b} - e \cos^2 \phi}} \sqrt{\frac{1 + e^2 \cos^2 \phi - e^2 \cos^4 \phi}{1 + \frac{1}{4} e^2 \sin^2 2\phi}} \left( \cos 2\alpha \cos 2\phi + \left(\frac{e}{2} + \frac{b}{a}\right) \sin 2\alpha \sin 2\phi \right) \quad (A.8) \\
&= 2R_G \dot{E} \frac{1}{\sqrt{\frac{a}{b} - e \cos^2 \phi}} \sqrt{\frac{1 + e^2 \cos^2 \phi (1 - \cos^2 \phi)}{1 + \frac{1}{4} e^2 \sin^2 2\phi}} \left( \cos 2\alpha \cos 2\phi + \left(\frac{e}{2} + \frac{b}{a}\right) \sin 2\alpha \sin 2\phi \right) \\
&= 2R_G \dot{E} \frac{1}{\sqrt{\frac{a}{b} - e \cos^2 \phi}} \left( \cos 2\alpha \cos 2\phi + \left(\frac{e}{2} + \frac{b}{a}\right) \sin 2\alpha \sin 2\phi \right)
\end{aligned}$$

Eq. (50) is obtained as follows.

$$\begin{aligned}
\Delta \dot{u}_t &= \Delta \dot{\mathbf{u}} \cdot \mathbf{t} \\
&= -2R\dot{E} \left( \cos 2\alpha \sin \theta \cos \beta - \sin 2\alpha \cos \theta \cos \beta \right. \\
&\quad \left. + \sin 2\alpha \sin \theta \sin \beta + \cos 2\alpha \cos \theta \sin \beta \right) \\
&= -2R\dot{E} \left[ \cos 2\alpha (\sin \theta \cos \beta + \cos \theta \sin \beta) \right. \\
&\quad \left. - \sin 2\alpha (\cos \theta \cos \beta - \sin \theta \sin \beta) \right] \quad (A.9) \\
&= -2R\dot{E} \left[ \cos 2\alpha \sin(\theta + \beta) - \sin 2\alpha \cos(\theta + \beta) \right]
\end{aligned}$$

$$\begin{aligned}
\Delta \dot{u}_t &= 2R\dot{E} \left[ \sin 2\alpha \frac{\cos 2\phi}{\sqrt{1 + \left(\frac{e}{2}\right)^2 \sin^2 2\phi}} - \cos 2\alpha \left(\frac{e}{2} + \frac{b}{a}\right) \sin 2\phi \frac{1}{\sqrt{1 + \left(\frac{e}{2}\right)^2 \sin^2 2\phi}} \right] \\
&= 2R_G \dot{E} \frac{\sqrt{\frac{b}{a} + e \cos^2 \phi}}{\sqrt{1 + \left(\frac{e}{2}\right)^2 \sin^2 2\phi}} \left[ \sin 2\alpha \cos 2\phi - \left(\frac{e}{2} + \frac{b}{a}\right) \cos 2\alpha \sin 2\phi \right] \\
&= 2R_G \dot{E} \frac{1}{\sqrt{\frac{a}{b} - e \cos^2 \phi}} \left[ \sin 2\alpha \cos 2\phi - \left(\frac{e}{2} + \frac{b}{a}\right) \cos 2\alpha \sin 2\phi \right]
\end{aligned} \tag{A.10}$$

### 3.1.2. $G_{12I}^{up+}$ and $G_{12I}^{tilt+}$ when lattice diffusion is dominant

Following standard theory of calculus with curvilinear coordinates (e.g. (Reddy, 2013)), the

basis vectors,  $\mathbf{g}_\rho$  and  $\mathbf{g}_\phi$ , of the curvilinear coordinate system defined by Eq. (46) are

$$\mathbf{g}_\rho = g_\rho \hat{\mathbf{g}}_\rho = \frac{\partial \mathbf{x}}{\partial \rho} = \left( \sqrt{\frac{b}{a}} \sin \phi, \sqrt{\frac{a}{b}} \cos \phi \right), \tag{A.11}$$

$$\mathbf{g}_\phi = g_\phi \hat{\mathbf{g}}_\phi = \frac{\partial \mathbf{x}}{\partial \phi} = \rho \left( \sqrt{\frac{b}{a}} \cos \phi, -\sqrt{\frac{a}{b}} \sin \phi \right), \tag{A.12}$$

where  $\hat{\mathbf{g}}_\rho$  and  $\hat{\mathbf{g}}_\phi$  are unit vectors. The norms,  $g_\rho$  and  $g_\phi$ , are

$$g_\rho = B(\phi) \tag{A.13}$$

$$g_\phi = \rho A(\phi) \tag{A.14}$$

Hence, according to Eqs (A.11) to (A.14), the differential of the position vector writes

$$d\mathbf{x} = B(\phi) d\rho \hat{\mathbf{g}}_\rho + \rho A(\phi) d\phi \hat{\mathbf{g}}_\phi \tag{A.15}$$

$\mathbf{g}_\phi$  is a divergence-free vector parallel to the tangent vector  $\mathbf{t}$ . The second term of Eq. (A.15) is

thus consistent with Eq. (41) expressing the curvilinear increment along the boundary.  $\mathbf{g}_\rho$  is

parallel to the radial vector  $\mathbf{R}$ , i.e.

$$\mathbf{n} \cdot \hat{\mathbf{g}}_\rho = \cos(\beta - \theta) = \frac{1}{A(\phi)B(\phi)} \quad (\text{A.16})$$

Hence, unless  $a = b$ , the coordinate system is non-orthogonal:

$$\mathbf{g}_\rho \cdot \mathbf{g}_\phi = -\rho \tan(\beta - \theta) = \rho C(\phi) \quad (\text{A.17})$$

$$\text{where } C(\phi) = -\frac{1}{2}e \sin 2\phi. \quad (\text{A.18})$$

Eqs. (A.16) and (A.17) are consistent with one another since

$$A(\phi)B(\phi) = \sqrt{1 + C^2(\phi)} \quad (\text{A.19})$$

Calculation of the upper bounds of  $\mathbf{G}_l$  under dominance of lattice diffusion requires a solution

for  $\mathbf{J}_l$  that complies both with boundary condition Eq. (60) and with condition  $\nabla \cdot \mathbf{J}_l = 0$  (Eq.

(20)). The solution can conveniently be written

$$\mathbf{J}_l = \dot{\mathbf{E}} \cdot \mathbf{x} + \lambda(\alpha) \mathbf{g}_\phi \quad (\text{A.20})$$

where  $\lambda(\alpha)$  is an arbitrary constant. Indeed, owing to the fact that  $\mathbf{g}_\phi$  is divergence free and

parallel to  $\mathbf{t}$ , boundary condition Eq. (60) follows from Eq. (27), whereas

$$\nabla \cdot \mathbf{J}_l = \nabla \cdot (\dot{\mathbf{E}} \cdot \mathbf{x}) = (\nabla \cdot \dot{\mathbf{E}}) \cdot \mathbf{x} + \dot{\mathbf{E}} : \nabla \mathbf{x} + \left( \frac{d\lambda}{d\alpha} \nabla \alpha \right) \cdot \mathbf{g}_\phi + \lambda \nabla \cdot \mathbf{g}_\phi = 0 \quad (\text{A.21})$$

since  $\alpha$  and  $\dot{\mathbf{E}}$  are uniform. From (A.20), the components  $J_{ln}$  and  $J_{lt}$  in directions normal and tangent to the boundary at  $\phi$  become, accounting for Eqs (49), (50), and (A.14),

$$j_{ln} = \mathbf{J}_l \cdot \mathbf{n} = \rho \dot{\mathbf{E}} \frac{1}{A(\phi)} (\cos 2\alpha \cos 2\phi + c \sin 2\alpha \sin 2\phi) \quad (\text{A.22})$$

$$j_{lt} = \mathbf{J}_l \cdot \mathbf{t} = \rho \dot{\mathbf{E}} \frac{1}{A(\phi)} (\sin 2\alpha \cos 2\phi - c \cos 2\alpha \sin 2\phi) + \rho A(\phi) \lambda(\alpha) \quad (\text{A.23})$$

According to Eq. (30), the contribution to  $\Psi$  due lattice diffusion is in this case

$$\Psi_l = \frac{1}{V} \int_V \frac{kT}{2\Omega D_l} \mathbf{J}_l \cdot \mathbf{J}_l dV = \frac{1}{V} \frac{kT}{2\Omega D_l} \int_0^{2\pi} \int_0^R r (J_{ln}^2 + J_{lt}^2) dr d\theta = \frac{1}{V} \frac{kT}{2\Omega D_l} \int_0^{2\pi} \int_0^{R_g} \rho (J_{ln}^2 + J_{lt}^2) d\rho d\phi \quad (\text{A.24})$$

In order that the solution for  $\mathbf{J}_l$  be as close as possible to the exact flux field, we calculate the value of  $\lambda(\alpha)$  that corresponds to a minimum of  $\Psi_l$ . The result is

$$\lambda(\alpha) = - \frac{\int_0^{2\pi} (\sin 2\alpha \cos 2\phi - c \cos 2\alpha \sin 2\phi) d\phi}{\int_0^{2\pi} A^2(\phi) d\phi} = 0 \quad (\text{A.25})$$

When  $\alpha = \frac{\pi}{4}$ , Eq. (A.24) then develops as follows:

$$\begin{aligned} \Psi_l &= \frac{1}{V} \frac{kT}{2\Omega D_l} \int_0^{2\pi} \int_0^{R_g} \rho (J_{ln}^2 + J_{lt}^2) d\rho d\phi \\ &= \frac{1}{\pi R_g^2} \frac{1}{2} \frac{kT}{\Omega D_l} \frac{R_g^4}{4} \dot{E}^2 \int_0^{2\pi} \left[ \frac{1}{A^2(\phi)} (c^2 \sin^2 2\phi + \cos^2 2\phi) \right] d\phi \end{aligned} \quad (\text{A.26})$$

$$\begin{aligned} c &= \frac{1}{2} \left( \frac{a}{b} + \frac{b}{a} \right) = \sqrt{1 + \left( \frac{e}{2} \right)^2} \\ c^2 \sin^2 2\phi + \cos^2 2\phi &= \left( \frac{e}{2} \right)^2 \sin^2 2\phi + 1 \end{aligned} \quad (\text{A.27})$$

$$\begin{aligned} 1 + \left( \frac{e}{2} \right)^2 \sin^2 2\phi &= \left( \frac{a}{b} - e \cos^2 \phi \right) \left( \frac{b}{a} + e \cos^2 \phi \right) = A^2(\phi) B^2(\phi) \\ \Psi_l &= \frac{1}{2\pi} \frac{kT R_g^2}{\Omega D_l} \frac{1}{4} \dot{E}^2 \int_0^{2\pi} \frac{1 + \left( \frac{e}{2} \right)^2 \sin^2 2\phi}{A^2(\phi)} d\phi \\ &= \frac{1}{2\pi} \frac{kT R_g^2}{\Omega D_l} \frac{1}{4} \dot{E}^2 \int_0^{2\pi} \left( \frac{b}{a} + e \cos^2 \phi \right) d\phi \\ &= \frac{1}{2\pi} \frac{kT R_g^2}{\Omega D_l} \frac{1}{4} \dot{E}^2 \left( \frac{b}{a} 2\pi + e\pi \right) \end{aligned} \quad (\text{A.28})$$

$$\text{i.e.} \quad \Psi_l = \frac{1}{4} c \frac{kTR_G^2}{\Omega D_l} \dot{\epsilon}^2 \quad (\text{A.29})$$

Quite remarkably,  $\Psi_l$  is the same for  $\alpha = \frac{\pi}{4}$  and  $\alpha = 0$ .  $G_{12l}^+$  derives from the sum

$\Psi = \Psi_l + \Psi_{sl}$  according to Eq. (32). Denoting  $\eta_l$  the non-dimensional boundary viscosity coefficient

$$\eta_l = \frac{\Omega D_l}{R_G kT} \eta = \frac{D_l}{R_G} \eta = \frac{R_G}{\delta} \frac{D_l}{D_b} \eta_b, \quad (\text{A.30})$$

$G_{12l}^{up+}$  and  $G_{12l}^{tilt+}$  then express as

$$G_{12l}^{up+} = \left( \frac{1}{8} c + \frac{1}{2} \eta_l \frac{1}{\pi} \int_0^{2\pi} \frac{\cos^2 2\phi}{A(\phi)} d\phi \right) \frac{R_G^2}{D_l} \quad (\text{A.31})$$

$$G_{12l}^{tilt+} = \left( \frac{1}{8} c + \frac{1}{2} \eta_l c^2 \frac{1}{\pi} \int_0^{2\pi} \frac{\sin^2 2\phi}{A(\phi)} d\phi \right) \frac{R_G^2}{D_l} \quad (\text{A.32})$$

### 3.2. Statical boundary conditions based on an uniform stress field

Eqs. (67) and (68) are obtained as follows :

$$\begin{aligned} \cos \beta &= \frac{1}{\sqrt{1 + \left( \frac{a}{b} \tan \phi \right)^2}} \\ \sin \beta &= \frac{1}{\sqrt{1 + \left( \frac{a}{b} \tan \phi \right)^{-2}}} \\ \cos(2\beta) &= -\sin^2 \beta + \cos^2 \beta \\ &= -\frac{1}{1 + \left( \frac{a}{b} \tan \phi \right)^{-2}} + \frac{1}{1 + \left( \frac{a}{b} \tan \phi \right)^2} \\ &= \frac{1 - \left( \frac{a}{b} \tan \phi \right)^2}{1 + \left( \frac{a}{b} \tan \phi \right)^2} \end{aligned} \quad (\text{A.33})$$

$$\begin{aligned}
1 + \left( \frac{a}{b} \tan \phi \right)^2 &= \frac{a}{b \cos^2 \phi} \left[ \frac{b}{a} \cos^2 \phi + \frac{a}{b} \sin^2 \phi \right] \\
&= \frac{a}{b \cos^2 \phi} \left[ \frac{a}{b} - \left( \frac{a}{b} - \frac{b}{a} \right) \cos^2 \phi \right] \\
&= \frac{a}{b \cos^2 \phi} \left[ \frac{a}{b} - e \cos^2 \phi \right] = \frac{a}{b \cos^2 \phi} A^2(\phi) \\
1 - \left( \frac{a}{b} \tan \phi \right)^2 &= \frac{a}{b \cos^2 \phi} \left[ \frac{b}{a} \cos^2 \phi - \frac{a}{b} \sin^2 \phi \right] \\
&= \frac{a}{b \cos^2 \phi} \left[ \frac{b}{a} \cos^2 \phi - \frac{b}{a} \sin^2 \phi - \left( \frac{a}{b} - \frac{b}{a} \right) \sin^2 \phi \right] \\
&= \frac{a}{b \cos^2 \phi} \left[ \frac{b}{a} \cos 2\phi + \frac{e}{2} (\cos 2\phi - 1) \right] \\
&= \frac{a}{b \cos^2 \phi} \left[ \left[ \frac{b}{a} + \frac{1}{2} \left( \frac{a}{b} - \frac{b}{a} \right) \right] \cos 2\phi - \frac{e}{2} \right] \\
&= \frac{a}{b \cos^2 \phi} \left[ \left[ \frac{1}{2} \left( \frac{a}{b} + \frac{b}{a} \right) \right] \cos 2\phi - \frac{e}{2} \right] \\
&= \frac{a}{b \cos^2 \phi} \left[ c \cos 2\phi - \frac{e}{2} \right]
\end{aligned} \tag{A.34}$$

$$\begin{aligned}
\cos(2\beta) &= \frac{1 - \left( \frac{a}{b} \tan \phi \right)^2}{1 + \left( \frac{a}{b} \tan \phi \right)^2} \\
&= \frac{c \cos 2\phi - \frac{e}{2}}{\frac{a}{b} - e \cos^2 \phi} = \frac{c \cos 2\phi - \frac{e}{2}}{A^2(\phi)}
\end{aligned} \tag{A.35}$$

$$\begin{aligned}
\cos \beta &= \frac{1}{\sqrt{1 + \left(\frac{a}{b} \tan \phi\right)^2}} \\
\sin \beta &= \frac{1}{\sqrt{1 + \left(\frac{a}{b} \tan \phi\right)^{-2}}} \\
\sin(2\beta) &= 2 \sin \beta \cos \beta \\
&= 2 \frac{1}{\sqrt{1 + \left(\frac{a}{b} \tan \phi\right)^{-2}} \sqrt{1 + \left(\frac{a}{b} \tan \phi\right)^2}} \\
&= 2 \frac{1}{\sqrt{2 + \left(\frac{a}{b} \tan \phi\right)^{-2} + \left(\frac{a}{b} \tan \phi\right)^2}} \\
&= \frac{\sin 2\phi}{\sqrt{2 \sin^2 \phi \cos^2 \phi + \left(\frac{b}{a}\right)^2 \cos^4 \phi + \left(\frac{a}{b}\right)^2 \sin^4 \phi}} \\
&= \frac{\sin 2\phi}{\frac{b}{a} \cos^2 \phi + \frac{a}{b} \sin^2 \phi} \\
&= \frac{\sin 2\phi}{\frac{a}{b} - \left(\frac{a}{b} - \frac{b}{a}\right) \cos^2 \phi} = \frac{\sin 2\phi}{A^2(\phi)}
\end{aligned} \tag{A.36}$$

Hence, finally,

$$\begin{aligned}
T_n &= S[\cos 2\alpha \cos 2\beta + \sin 2\alpha \sin 2\beta] \\
&= S \frac{1}{A^2(\phi)} \left[ \cos 2\alpha \left( c \cos 2\phi - \frac{e}{2} \right) + \sin 2\alpha \sin 2\phi \right]
\end{aligned} \tag{A.37}$$

$$\begin{aligned}
T_t &= S[\sin 2\alpha \cos 2\beta - \cos 2\alpha \sin 2\beta] \\
&= -S \frac{1}{A^2(\phi)} \left[ \cos 2\alpha \sin 2\phi - \sin 2\alpha \left( c \cos 2\phi - \frac{e}{2} \right) \right]
\end{aligned} \tag{A.38}$$



Via Eqs.(33), the contribution to  $\Phi$  due to grain boundary sliding,  $\Phi_{sl}$ , is easily derived from

Eq. (68):

$$\begin{aligned}\Phi_{sl} &= \frac{1}{V_S} \int \frac{1}{2\eta} T_t^2 ds \\ &= \frac{1}{\pi R_G} \frac{1}{4\eta} S^2 \int_0^{2\pi} \frac{1}{A^3(\phi)} \left[ \cos 2\alpha \sin 2\phi - \sin 2\alpha \left( c \cos 2\phi - \frac{e}{2} \right) \right]^2 d\phi\end{aligned}\quad (\text{A.39})$$

### 3.2.1. $G_{12b}^{up-}$ and $G_{12b}^{tilt-}$ when grain boundary diffusion is dominant

When grain boundary diffusion is dominant the surface gradient of diffusion potential,  $\nabla_s \mu$ , is obtained from Eqs. (22) and (67) as

$$\nabla_s \mu = \frac{dT_n}{ds} \quad (\text{A.40})$$

which develops as follows:

$$\begin{aligned}T_n &= S \frac{1}{\frac{a}{b} - e \cos^2 \phi} \left( \cos 2\alpha \left( c \cos 2\phi - \frac{e}{2} \right) + \sin 2\alpha \sin 2\phi \right) \\ \frac{dT_n}{ds} &= \frac{dT_n}{d\phi} \frac{1}{R_G \sqrt{\frac{a}{b} - e \cos^2 \phi}} \\ &= S \frac{1}{R_G \sqrt{\frac{a}{b} - e \cos^2 \phi}} \frac{1}{\left( \frac{a}{b} - e \cos^2 \phi \right)^2} \left[ \begin{aligned} &\cos 2\alpha \left[ \begin{aligned} &-2c \sin 2\phi \left( \frac{a}{b} - e \cos^2 \phi \right) \\ &-(2e \sin \phi \cos \phi) \left( c \cos 2\phi - \frac{e}{2} \right) \end{aligned} \right] \\ &+ \sin 2\alpha \left[ \begin{aligned} &2 \cos 2\phi \left( \frac{a}{b} - e \cos^2 \phi \right) \\ &-(2e \sin \phi \cos \phi) \sin 2\phi \end{aligned} \right] \end{aligned} \right] \\ &= S \frac{1}{R_G} \frac{1}{\left( \frac{a}{b} - e \cos^2 \phi \right)^{\frac{5}{2}}} \left[ \begin{aligned} &\cos 2\alpha \sin 2\phi \left( -2c \left( \frac{a}{b} - e \cos^2 \phi \right) - e \left( c \cos 2\phi - \frac{e}{2} \right) \right) \\ &+ \sin 2\alpha \left[ 2 \cos 2\phi \left( \frac{a}{b} - e \cos^2 \phi \right) - e \sin^2 2\phi \right] \end{aligned} \right] \quad (\text{A.41})\end{aligned}$$

$$\begin{aligned}
T_n &= S \frac{1}{R_G} \frac{1}{\left(\frac{a}{b} - e \cos^2 \phi\right)^{\frac{5}{2}}} \left[ \begin{aligned} &\cos 2\alpha \sin 2\phi \left[ -2c \left( \frac{a}{b} - e \cos^2 \phi \right) \right. \\ &\quad \left. - e \left( c(2 \cos^2 \phi - 1) - \frac{e}{2} \right) \right] \\ &+ \sin 2\alpha \cos 2\phi \left[ 2 \left( \frac{a}{b} - e \cos^2 \phi \right) - e \frac{\sin^2 2\phi}{\cos 2\phi} \right] \end{aligned} \right] \\
&= S \frac{1}{R_G} \frac{1}{\left(\frac{a}{b} - e \cos^2 \phi\right)^{\frac{5}{2}}} \left[ \begin{aligned} &\cos 2\alpha \sin 2\phi \left[ -2c \frac{a}{b} + ec + \frac{e^2}{2} + (2ce - 2ec) \cos^2 \phi \right] \\ &+ \sin 2\alpha \cos 2\phi \left[ 2 \left( \frac{a}{b} - e \cos^2 \phi \right) - e \frac{\sin^2 2\phi}{\cos 2\phi} \right] \end{aligned} \right] \quad (\text{A.42}) \\
&= S \frac{1}{R_G} \frac{1}{\left(\frac{a}{b} - e \cos^2 \phi\right)^{\frac{5}{2}}} \left[ \begin{aligned} &\cos 2\alpha \sin 2\phi \left[ -2c \frac{a}{b} + ec + \frac{e^2}{2} \right] \\ &+ \sin 2\alpha \cos 2\phi \left[ 2 \left( \frac{a}{b} - e \cos^2 \phi \right) - e \frac{\sin^2 2\phi}{\cos 2\phi} \right] \end{aligned} \right]
\end{aligned}$$

$$\begin{aligned}
c^2 &= 1 + \left( \frac{e}{2} \right)^2 \\
ce &= e \sqrt{1 + \left( \frac{e}{2} \right)^2} \\
c + \frac{e}{2} &= \frac{1}{2} \left( \frac{a}{b} + \frac{b}{a} \right) + \frac{1}{2} \left( \frac{a}{b} - \frac{b}{a} \right) = \frac{a}{b} \\
\frac{e}{2} - c &= \frac{1}{2} \left( \frac{a}{b} - \frac{b}{a} \right) - \frac{1}{2} \left( \frac{a}{b} + \frac{b}{a} \right) = -\frac{b}{a} \\
-2c \frac{a}{b} + ec + \frac{e^2}{2} &= -2c \frac{a}{b} + e \frac{a}{b} = 2 \frac{a}{b} \left( \frac{e}{2} - c \right) = -2
\end{aligned} \quad (\text{A.43})$$

$$\begin{aligned}
\frac{dT_n}{ds} &= \frac{dT_n}{d\phi} \frac{1}{R_G \sqrt{\frac{a}{b} - e \cos^2 \phi}} \\
&= S \frac{1}{R_G} \frac{1}{\left(\frac{a}{b} - e \cos^2 \phi\right)^{\frac{5}{2}}} \left[ \begin{aligned} &\cos 2\alpha \sin 2\phi \left[ -2c \frac{a}{b} + ec + \frac{e^2}{2} \right] \\ &+ \sin 2\alpha \cos 2\phi \left[ 2 \left( \frac{a}{b} - e \cos^2 \phi \right) - e \frac{\sin^2 2\phi}{\cos 2\phi} \right] \end{aligned} \right] \quad (\text{A.44}) \\
&= -2S \frac{1}{R_G} \frac{1}{A^5(\phi)} \left[ \begin{aligned} &\cos 2\alpha \sin 2\phi \\ &- \sin 2\alpha \cos 2\phi \left( A^2(\phi) - \frac{e \sin^2 2\phi}{2 \cos 2\phi} \right) \end{aligned} \right]
\end{aligned}$$

One obtains finally

$$\begin{aligned}\nabla_s \mu &= \frac{dT_n}{ds} \\ &= -2 \frac{1}{R_G} S \frac{1}{A^5(\phi)} \left[ \cos 2\alpha \sin 2\phi - \sin 2\alpha \cos 2\phi \left( A^2(\phi) - \frac{e \sin^2 2\phi}{2 \cos 2\phi} \right) \right]\end{aligned}\quad (\text{A.45})$$

and Eq. (33) becomes

$$\begin{aligned}\Phi_b &= \frac{1}{2V} \int_S \frac{\delta D_b}{2\Omega kT} \nabla_s \mu \cdot \nabla_s \mu ds \\ &= \frac{1}{\pi} \frac{1}{R_G^3} S^2 \frac{\delta D_b}{\Omega kT} \int_0^{2\pi} \frac{1}{A^9(\phi)} \left[ \cos 2\alpha \sin 2\phi - \sin 2\alpha \cos 2\phi \left( A^2(\phi) - \frac{e \sin^2 2\phi}{2 \cos 2\phi} \right) \right]^2 d\phi\end{aligned}\quad (\text{A.46})$$

$G_{12b}^-$  derives from the sum  $\Phi = \Phi_b + \Phi_{sl}$  according to Eq.(35). For  $\alpha = \frac{\pi}{4}$ , Eqs (A.39) and

(A.46) yield

$$\frac{1}{G_{12b}^{up-}} = \left[ \frac{2}{\pi} \int_0^{2\pi} \frac{\cos^2 2\phi}{A^9(\phi)} \left( A^2(\phi) - \frac{e \sin^2 2\phi}{2 \cos 2\phi} \right)^2 d\phi + \frac{1}{2} \frac{1}{\eta_b} \frac{1}{\pi} \int_0^{2\pi} \frac{\left( c \cos 2\phi - \frac{e}{2} \right)^2}{A^3(\phi)} d\phi \right] \frac{\mathcal{D}_b}{R_G^3} \quad (\text{A.47})$$

and for  $\alpha = 0$

$$\frac{1}{G_{12b}^{tilt-}} = \left( \frac{2}{\pi} \int_0^{2\pi} \frac{\sin^2 2\phi}{A^9(\phi)} d\phi + \frac{1}{2} \frac{1}{\eta_b} \frac{1}{\pi} \int_0^{2\pi} \frac{\sin^2 2\phi}{A^3(\phi)} d\phi \right) \frac{\mathcal{D}_b}{R_G^3}. \quad (\text{A.48})$$

### 3.2.2. $G_{12l}^{up-}$ and $G_{12l}^{tilt-}$ when lattice diffusion is dominant

The coupling of Eqs. (19) and (67) yields

$$(\mu)_{\rho=R_G} = \mu^o - \Omega S \frac{1}{A^2(\phi)} \left[ \cos 2\alpha \left( c \cos 2\phi - \frac{e}{2} \right) + \sin 2\alpha \sin 2\phi \right] \quad (\text{A.49})$$

A trial field satisfying boundary condition (A.49) is

$$\mu = \mu^\circ - \Omega S \frac{\rho^2}{R_G^2} \left( \frac{\cos 2\alpha \left( c \cos 2\phi - \frac{e}{2} \right) + \sin 2\alpha \sin 2\phi}{A^2(\phi)} + \gamma \right) + \gamma \Omega S \quad (\text{A.50})$$

where  $\gamma$  is an adjustable parameter which is taken not to be dependent on  $\rho$  and  $\phi$ .

The contribution of lattice diffusion to potential  $\Phi$  can be calculated using

$$\Phi_l = \frac{1}{V} \frac{D_l}{2\Omega kT} \int_0^{2\pi} \int_0^R r (\nabla \mu \cdot \nabla \mu) dr d\theta = \frac{1}{V} \frac{D_l}{2\Omega kT} \int_0^{2\pi} \int_0^{R_G} \rho (\nabla \mu \cdot \nabla \mu) d\rho d\phi \quad (\text{A.51})$$

and  $G_{12l}^-$  can be derived in turn from the sum  $\Phi = \Phi_l + \Phi_{sl}$  according to Eq.(35). In order to

calculate  $\nabla \mu$  we introduce the set of reciprocal basis vectors defined by

$$\mathbf{g}^\rho = g^\rho \hat{\mathbf{g}}^\rho = \frac{\partial \rho}{\partial \mathbf{x}_1} \hat{\mathbf{x}}_1 + \frac{\partial \rho}{\partial \mathbf{x}_2} \hat{\mathbf{x}}_2 = \left( \sqrt{\frac{a}{b}} \sin \phi, \sqrt{\frac{b}{a}} \cos \phi \right), \quad (\text{A.52})$$

$$\mathbf{g}^\phi = g^\phi \hat{\mathbf{g}}^\phi = \frac{\partial \phi}{\partial \mathbf{x}_1} \hat{\mathbf{x}}_1 + \frac{\partial \phi}{\partial \mathbf{x}_2} \hat{\mathbf{x}}_2 = \frac{1}{\rho} \left( \sqrt{\frac{a}{b}} \cos \phi, -\sqrt{\frac{b}{a}} \sin \phi \right), \quad (\text{A.53})$$

which means

$$g^\rho = A(\phi) \quad (\text{A.54})$$

$$g^\phi = \frac{1}{\rho} B(\phi) \quad (\text{A.55})$$

$\mathbf{g}^\rho$  is parallel to the normal vector  $\mathbf{n}$  whereas

$$\mathbf{t} \cdot \hat{\mathbf{g}}^\phi = \cos(\beta - \theta) = \frac{1}{A(\phi) B(\phi)} \quad (\text{A.56})$$

$\hat{\mathbf{g}}^\rho$  and  $\hat{\mathbf{g}}_\phi$  are thus, respectively, alternative notations for unit vectors  $\mathbf{n}$  and  $\mathbf{t}$  at given  $\phi$ .

The gradient of the diffusion potential can be expressed on the basis of reciprocal basis vectors as

$$\nabla\mu = \frac{\partial\mu}{\partial\rho}\mathbf{g}^\rho + \frac{\partial\mu}{\partial\phi}\mathbf{g}^\phi = A(\phi)\frac{\partial\mu}{\partial\rho}\hat{\mathbf{g}}^\rho + \frac{1}{\rho}B(\phi)\frac{\partial\mu}{\partial\phi}\hat{\mathbf{g}}^\phi \quad (\text{A.57})$$

Using Eq. (A.56), one can develop the following:

$$\begin{aligned} \sin(\beta - \theta) &= \cos\theta \sin\beta - \sin\theta \cos\beta \\ &= \frac{1}{\sqrt{1+\left(\frac{b}{a}\tan\phi\right)^2}} \frac{1}{\sqrt{1+\left(\frac{a}{b}\tan\phi\right)^{-2}}} - \frac{1}{\sqrt{1+\left(\frac{b}{a}\tan\phi\right)^{-2}}} \frac{1}{\sqrt{1+\left(\frac{a}{b}\tan\phi\right)^2}} \\ &= \frac{1}{\sqrt{1+\left(\frac{b}{a}\right)^4 + \left(\frac{a}{b}\tan\phi\right)^{-2} + \left(\frac{b}{a}\tan\phi\right)^2}} \\ &\quad - \frac{1}{\sqrt{1+\left(\frac{a}{b}\right)^4 + \left(\frac{b}{a}\tan\phi\right)^{-2} + \left(\frac{a}{b}\tan\phi\right)^2}} \\ &= \frac{1}{\sqrt{1+\left(\frac{b}{a}\right)^4 + \left(\frac{a}{b}\tan\phi\right)^{-2} + \left(\frac{b}{a}\tan\phi\right)^2}} \left(1 - \frac{b^2}{a^2}\right) \\ &= \frac{1}{\sqrt{\left(1+\left(\frac{b}{a}\right)^4\right)\left(\frac{a}{b}\tan\phi\right)^2 + 1 + \left(\frac{b}{a}\tan\phi\right)^2\left(\frac{a}{b}\tan\phi\right)^2}} \left(1 - \frac{b^2}{a^2}\right) \frac{a}{b} \tan\phi \\ &= \frac{1}{\sqrt{1+\left(\frac{b^2}{a^2} + \frac{a^2}{b^2}\right)\tan^2\phi + \tan^4\phi}} \left(\frac{a}{b} - \frac{b}{a}\right) \tan\phi \\ &= \frac{1}{2} e \sin 2\phi \frac{1}{\sqrt{\cos^4\phi + \left(\frac{b^2}{a^2} + \frac{a^2}{b^2}\right)\sin^2\phi \cos^2\phi + \sin^4\phi}} \\ &= \frac{1}{2} e \sin 2\phi \frac{1}{\sqrt{\cos^4\phi + \left(\frac{b^2}{a^2} + \frac{a^2}{b^2}\right)\sin^2\phi \cos^2\phi + \sin^4\phi}} \\ &= \frac{e}{2} \sin 2\phi \frac{1}{\sqrt{1+\left(\frac{e}{2}\right)^2 \sin^2 2\phi}} \end{aligned} \quad (\text{A.58})$$

Hence, owing to the equality  $\sqrt{1 + \left(\frac{e}{2}\right)^2 \sin^2 2\phi} = \sqrt{\frac{a}{b} - e \cos^2 \phi} \sqrt{\frac{b}{a} + e \cos^2 \phi}$ ,

$$\sin(\beta - \theta) = \frac{e}{2} \frac{\sin 2\phi}{A(\phi)B(\phi)} \quad (\text{A.59})$$

Eq. (A.57) thus convert into

$$\begin{aligned} \nabla \mu \cdot \nabla \mu &= \nabla \mu^{\rho^2} + \nabla \mu^{\phi^2} + 2 \nabla \mu^\rho \nabla \mu^\phi \sin(\beta - \theta) \\ &= \nabla \mu^{\rho^2} + \nabla \mu^{\phi^2} + \frac{e}{A(\phi)B(\phi)} \nabla \mu^\rho \nabla \mu^\phi \sin 2\phi \end{aligned} \quad (\text{A.60})$$

Alternatively, Eq. (A.60) can be obtained as follows

$$\begin{aligned} \nabla \mu &= \frac{\partial \mu}{\partial x_1} \hat{\mathbf{x}}_1 + \frac{\partial \mu}{\partial x_2} \hat{\mathbf{x}}_2 \\ \frac{\partial \mu}{\partial x_1} &= \frac{\partial \mu}{\partial \rho} \frac{\partial \rho}{\partial x_1} + \frac{\partial \mu}{\partial \phi} \frac{\partial \phi}{\partial x_1} = \sqrt{\frac{a}{b}} \sin \phi \frac{\partial \mu}{\partial \rho} + \frac{1}{\rho} \sqrt{\frac{a}{b}} \cos \phi \frac{\partial \mu}{\partial \phi} \end{aligned} \quad (\text{A.61})$$

$$\frac{\partial \mu}{\partial x_2} = \frac{\partial \mu}{\partial \rho} \frac{\partial \rho}{\partial x_2} + \frac{\partial \mu}{\partial \phi} \frac{\partial \phi}{\partial x_2} = \sqrt{\frac{b}{a}} \cos \phi \frac{\partial \mu}{\partial \rho} - \frac{1}{\rho} \sqrt{\frac{b}{a}} \sin \phi \frac{\partial \mu}{\partial \phi}$$

$$\begin{aligned} \left( \frac{\partial \mu}{\partial x_1} \right)^2 + \left( \frac{\partial \mu}{\partial x_2} \right)^2 &= \left( \frac{a}{b} \sin^2 \phi + \frac{b}{a} \cos^2 \phi \right) \left( \frac{\partial \mu}{\partial \rho} \right)^2 \\ &\quad + \frac{1}{\rho^2} \left( \frac{a}{b} \cos^2 \phi + \frac{b}{a} \sin^2 \phi \right) \left( \frac{\partial \mu}{\partial \phi} \right)^2 \\ &\quad + \frac{2}{\rho} \sin \phi \cos \phi \left( \frac{a}{b} - \frac{b}{a} \right) \frac{\partial \mu}{\partial \rho} \frac{\partial \mu}{\partial \phi} \end{aligned} \quad (\text{A.62})$$

$$\begin{aligned} \left( \frac{\partial \mu}{\partial x_1} \right)^2 + \left( \frac{\partial \mu}{\partial x_2} \right)^2 &= \left( \frac{a}{b} - e \cos^2 \phi \right) \left( \frac{\partial \mu}{\partial \rho} \right)^2 + \frac{1}{\rho^2} \left( \frac{b}{a} + e \cos^2 \phi \right) \left( \frac{\partial \mu}{\partial \phi} \right)^2 \\ &\quad + 2 \frac{1}{\rho} e \sin \phi \cos \phi \frac{\partial \mu}{\partial \rho} \frac{\partial \mu}{\partial \phi} \end{aligned}$$

Let us consider successively upright and tilted orientations. If  $\alpha = \frac{\pi}{4}$ , Eqs. (A.50) and (A.57)

yield

$$\nabla \mu^{\rho up} = -2\Omega S \frac{\rho}{R_G^2} \left( \frac{\sin 2\phi}{A(\phi)} + A(\phi) \gamma^{up} \right) \quad (\text{A.63})$$

$$\begin{aligned} \nabla \mu^\phi &= -\Omega S \frac{\rho}{R_G^2} B(\phi) \frac{\partial}{\partial \phi} \left( \frac{\sin 2\phi}{A^2(\phi)} \right) \\ \frac{\partial}{\partial \phi} \left( \frac{\sin 2\phi}{A^2(\phi)} \right) &= \frac{R_G}{S} A(\phi) \frac{dT_n}{ds} \\ &= \frac{R_G}{S} A(\phi) 2S \frac{1}{R_G} \frac{1}{A^5(\phi)} \cos 2\phi \left( A^2(\phi) - \frac{e \sin^2 2\phi}{2 \cos 2\phi} \right) \\ &= 2 \frac{1}{A^4(\phi)} \cos 2\phi \left( A^2(\phi) + \frac{e \sin^2 2\phi}{2 \cos 2\phi} \right) \end{aligned} \quad (\text{A.64})$$

$$\nabla \mu^{\phi up} = -2\Omega S \frac{\rho}{R_G^2} \frac{B(\phi)}{A^4(\phi)} \cos 2\phi \left( A^2(\phi) - \frac{e \sin^2 2\phi}{2 \cos 2\phi} \right) \quad (\text{A.65})$$

In order that the trial diffusion potential field be as close as possible to the exact field, we

search for an optimum by calculating the value of  $\gamma^{up}$  that yields a minimum of the potential

$\dot{\Phi}_I$ , expressed by Eq. (A.51). Via Eq. (A.60) one obtains

$$\gamma^{up} = - \frac{\int_0^{2\pi} \left[ \sin 2\phi + \frac{1}{4} e \sin 4\phi \frac{1}{A^4(\phi)} \left( A^2(\phi) - \frac{e \sin^2 2\phi}{2 \cos 2\phi} \right) \right] d\phi}{\int_0^{2\pi} A^2(\phi) d\phi} = 0 \quad (\text{A.66})$$

and

$$\begin{aligned} \Phi_I^{up} &= \frac{1}{2} \frac{1}{\pi} \frac{D_I \Omega}{k T R_G^2} S^2 \int_0^{2\pi} \left[ \frac{\sin^2 2\phi}{A^2(\phi)} + \frac{B^2(\phi)}{A^8(\phi)} \cos^2 2\phi \left( A^2(\phi) - \frac{e \sin^2 2\phi}{2 \cos 2\phi} \right)^2 \right. \\ &\quad \left. + \frac{1}{2} e \frac{\sin 4\phi \sin 2\phi}{A^6(\phi)} \left( A^2(\phi) - \frac{e \sin^2 2\phi}{2 \cos 2\phi} \right) \right] d\phi \end{aligned} \quad (\text{A.67})$$

Notice that the fact that  $\gamma^{up} = 0$  could hardly have been anticipated from consideration of symmetry. Conversely, if  $\alpha = 0$ ,

$$\gamma^{tilt} = - \frac{\int_0^{2\pi} \left( c \cos 2\phi - \frac{e}{2} - \frac{1}{2} e \frac{\sin^2 2\phi}{A^4(\phi)} \right) d\phi}{\int_0^{2\pi} A^2(\phi) d\phi} \neq 0 \quad (\text{A.68})$$

and

$$\begin{aligned} \Phi_I^{tilt} = \frac{1}{2} \frac{1}{\pi} \frac{D_I \Omega}{k T R_G^2} S^2 \int_0^{2\pi} & \left[ \left( \frac{c \cos 2\phi - \frac{e}{2}}{A(\phi)} + A(\phi) \gamma^{tilt} \right)^2 + \frac{B^2(\phi)}{A^8(\phi)} \sin^2 2\phi \right. \\ & \left. - e \frac{\sin^2 2\phi}{A^5(\phi)} \left( \frac{c \cos 2\phi - \frac{e}{2}}{A(\phi)} + A(\phi) \gamma^{tilt} \right) \right] d\phi \end{aligned} \quad (\text{A.69})$$

It can be verified that minima of  $\Phi_I^{up}$  and  $\Phi_I^{tilt}$  are obtained when  $\gamma^{up}$  and  $\gamma^{tilt}$  are given the values of Eqs. (A.66) and (A.68).

In view of the complexity of the development, we have found useful to verify the correctness of Eqs. (A.67) and (A.69) by numerical computations using Cartesian coordinates. For example, if

$\frac{a}{b} = 2$ , Eq. (84) expresses in Cartesian coordinates

$$\mu = \mu^o - \Omega S \frac{1}{R_G^2} \left( 2x_1^2 + \frac{1}{2} x_2^2 \right) \left( -\frac{4x_1^2 - \frac{1}{4} x_2^2}{4x_1^2 + \frac{1}{4} x_2^2} + \gamma \right) + \gamma \Omega S. \quad (\text{A.70})$$

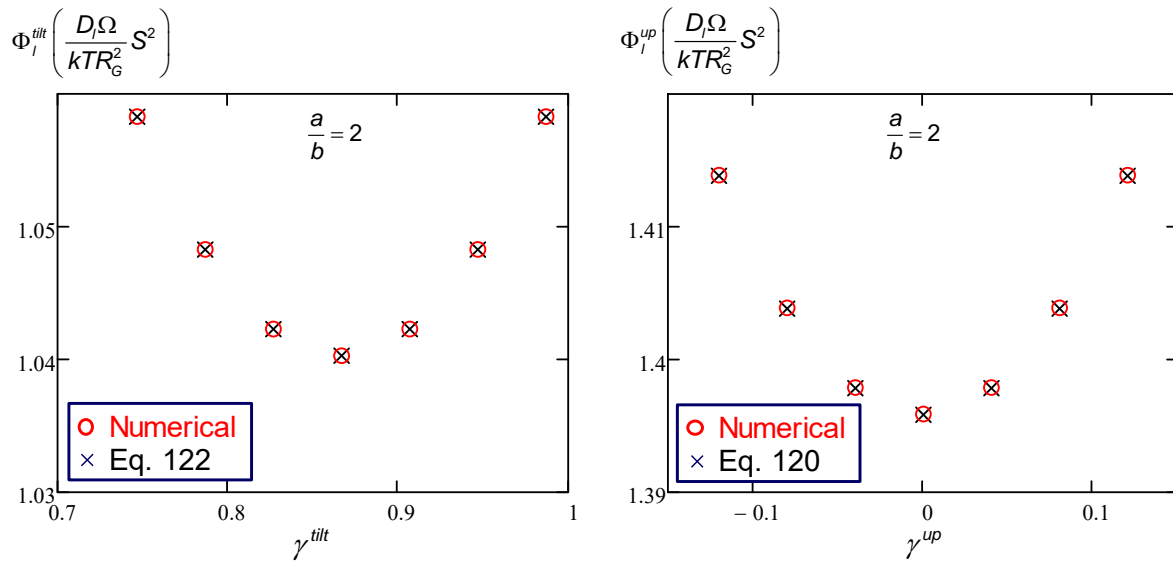
From this expression,  $\Phi_I^{up}$  and  $\Phi_I^{tilt}$  can be obtained numerically via

$$\Phi_I = \frac{1}{V} \frac{D_I}{2\Omega k T} \int_V \nabla \mu \cdot \nabla \mu dv = \frac{1}{V} \frac{D_I}{2\Omega k T} \int_{-\sqrt{2}}^{\sqrt{2}} \left( \int_{-\sqrt{2-x_2^2}}^{\sqrt{2-x_2^2}} \nabla \mu \cdot \nabla \mu dx_1 \right) dx_2 \quad (\text{A.71})$$



It has been verified that the  $\Phi_I^{up}$  and  $\Phi_I^{tilt}$  values obtained by full numerical computation of this latter equation are the exactly identical to the values obtained via Eqs. (A.67) and (A.69).

This is illustrated for the case  $\frac{a}{b} = 2$  in the following figure, which also shows the variation of  $\Phi_I^{up}$  and  $\Phi_I^{tilt}$  in the vicinity of the optimum value of  $\gamma^{up}$  and  $\gamma^{tilt}$ . A departure of 10% from the optimum value brings about an increase of  $\Phi_I^{up}$  and  $\Phi_I^{tilt}$  by about 1.5 %.



Using Eqs. (A.39), (A.67) and (A.69),  $G_{12I}^{up-}$  and  $G_{12I}^{tilt-}$  are finally obtained as

$$\frac{1}{G_{12I}^{up-}} = \left\{ \frac{1}{\pi} \int_0^{2\pi} \left[ \frac{\sin^2 2\phi}{A^2(\phi)} + \frac{B^2(\phi)}{A^8(\phi)} \cos^2 2\phi \left( A^2(\phi) - \frac{e \sin^2 2\phi}{2 \cos 2\phi} \right)^2 \right. \right. \\ \left. \left. + \frac{1}{2} e \frac{\sin 4\phi \sin 2\phi}{A^6(\phi)} \left( A^2(\phi) - \frac{e \sin^2 2\phi}{2 \cos 2\phi} \right) \right] d\phi + \frac{1}{2} \frac{1}{\eta_I} \frac{1}{\pi} \int_0^{2\pi} \frac{\left( c \cos 2\phi - \frac{e}{2} \right)^2}{A^3(\phi)} d\phi \right\} \left\{ \frac{D_I}{R_G^2} \right\} \quad (A.72)$$

and

$$\begin{aligned} \frac{1}{G_{12l}^{tilt-}} = & \left\{ \frac{1}{\pi} \int_0^{2\pi} \left[ \left( \frac{c \cos 2\phi - \frac{e}{2}}{A(\phi)} + A(\phi) \gamma^{tilt} \right)^2 + \frac{B^2(\phi)}{A^8(\phi)} \sin^2 2\phi \right. \right. \\ & \left. \left. - e \frac{\sin^2 2\phi}{A^5(\phi)} \left( \frac{c \cos 2\phi - \frac{e}{2}}{A(\phi)} + A(\phi) \gamma^{tilt} \right) \right] d\phi + \frac{1}{2} \frac{1}{\eta_l} \frac{1}{\pi} \int_0^{2\pi} \frac{\sin^2 2\phi}{A^3(\phi)} d\phi \right\} \frac{\mathcal{D}_l}{R_G^2} \end{aligned} \quad (A.73)$$

#### 4. Discussion

*Statical bound  $G_{b_{hexag.}}^-$  for a hexagonal grain*

The grain is now represented as having a regular polygonal cross-section with an area  $\pi R_G^2$ .

The equations are developed for an arbitrary integer grain coordination  $Z \geq 3$  (hence, for illustration,  $Z = 7$  in Fig. A1). Restriction to  $Z = 6$  is made at the end.

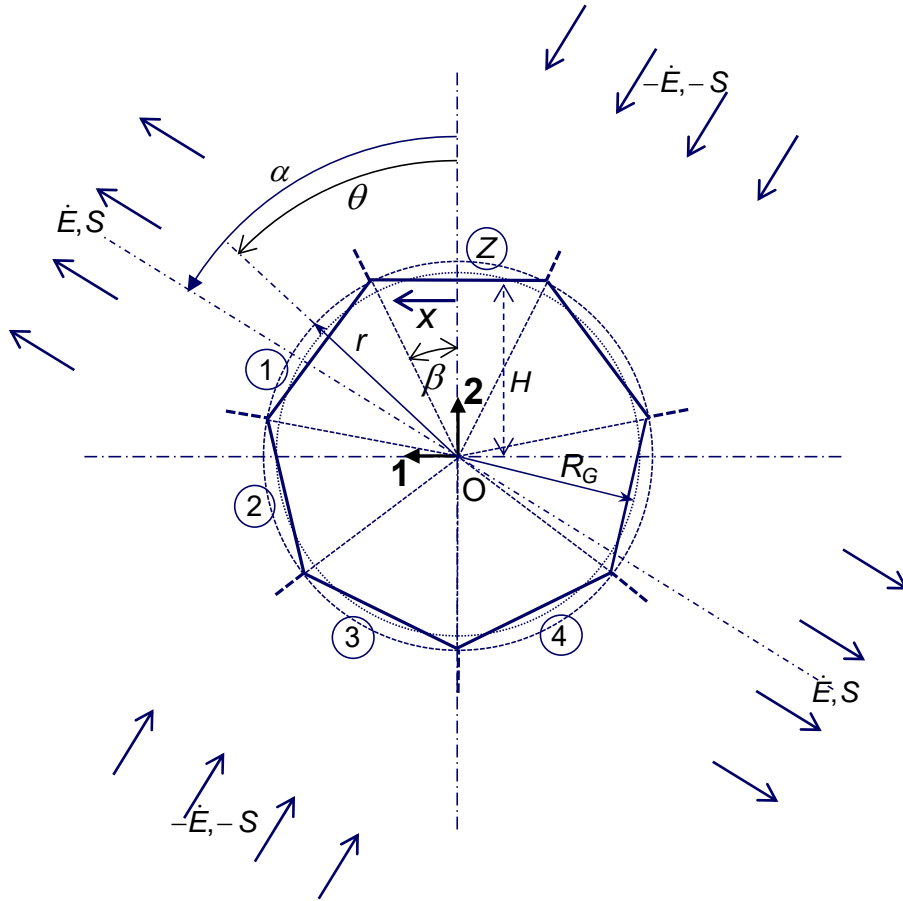


Figure A1: Grain with regular polygonal cross-section

The grain is a collection of  $Z$  identical triangles of which the aperture angle at  $O$  is

$$2\beta = \frac{2\pi}{Z} \quad (\text{A.74})$$

$r$  denotes the radius of the circle circumscribing the polygon. It is related to average grain size via

$$R_G = r \left( \frac{\sin \beta \cos \beta}{\beta} \right)^{\frac{1}{2}} \quad (\text{A.75})$$

The height,  $H$ , of the  $Z$  triangles is

$$H = r \cos \beta = R_G \left( \frac{\beta}{\tan \beta} \right)^{\frac{1}{2}} \quad (\text{A.76}).$$

Faces are designated by subscript  $m$  with  $1 \leq m \leq Z$ . Face  $m = Z$  is perpendicular to axis **2** ( $m$

$=1 \equiv m = Z + 1$ ). The coordinate from the middle of the face is thus  $x = r \sin(\theta - 2m\beta)$  with  $-\beta \leq \theta - 2m\beta \leq \beta$ . Unit vectors  $\mathbf{n}$  and  $\mathbf{t}$  normal and tangent to grain faces are

$$\begin{bmatrix} n_{1m} \\ n_{2m} \end{bmatrix} = \begin{bmatrix} \sin(2m\beta) \\ \cos(2m\beta) \end{bmatrix} \quad (\text{A.77})$$

and  $\begin{bmatrix} t_{1m} \\ t_{2m} \end{bmatrix} = \begin{bmatrix} \cos(2m\beta) \\ -\sin(2m\beta) \end{bmatrix}$  (A.78)

We consider the macroscopic stress tensor

$$\mathbf{S} = S \begin{bmatrix} -\cos 2\alpha & \sin 2\alpha \\ \sin 2\alpha & \cos 2\alpha \end{bmatrix}. \quad (\text{A.79})$$

Uniform stress boundary conditions means that the average of the tractions in a face is

$$T_{iav.m} = S_{ij} n_{jm} \quad (\text{A.80})$$

which yields

$$\begin{bmatrix} T_{1av.m} \\ T_{2av.m} \end{bmatrix} = S \begin{bmatrix} \sin(2\alpha - 2m\beta) \\ \cos(2\alpha - 2m\beta) \end{bmatrix} \quad (\text{A.81})$$

and  $T_{nav.m} = S \cos[2\alpha - 4m\beta]$  (A.82)

$$T_{tav.m} = S \sin[2\alpha - 4m\beta] \quad (\text{A.83})$$

Owing to grain rigidity,  $T_{tm}$  is uniform along a grain face:

$$T_{tm} = T_{tav.m} = S \sin(2\alpha - 4m\beta) \quad (\text{A.84})$$

Hence  $\Delta \dot{u}_{tm} = \frac{S}{\eta} \sin(2\alpha - 4m\beta)$  (A.85)

and the dissipation rate due to grain boundary sliding is,

$$\begin{aligned}\dot{Q}_{sl.} &= \frac{1}{V} \frac{1}{2} \sum_{m=1}^{m=Z} \int_{-r \sin \beta}^{r \sin \beta} \eta (\Delta \dot{u}_{tm})^2 dx \\ &= \frac{1}{2} S^2 \frac{1}{\eta_b} \frac{\mathcal{D}}{R_G^3} \left( \frac{\sin \beta}{\beta} \right)^{\frac{1}{2}} \cos^{\frac{1}{2}} \beta = \frac{1}{2} \left( \frac{2\sqrt{3}}{\pi} \right)^{\frac{1}{2}} S^2 \frac{1}{\eta_b} \frac{\mathcal{D}}{R_G^3}\end{aligned}\quad (\text{A.86})$$

Local normal tractions  $T_{nm}(x)$  can be expressed in terms of departure from the average  $T_{nav.m}$ .

If faces remain parallel,  $T_{nm}$  is parabolic :

$$T_{nm} = T_{nav.m} - \frac{S}{r^2} \left[ (a' x^2 + d' r^2) \cos(2\alpha - 4m\beta) \right] \quad (\text{A.87})$$

where  $a'$  and  $d'$  are non-dimensional parameters. Diffusion flux and velocity jump thus express as

$$j_m = -\mathcal{D} \frac{S}{r^2} (2a' x \cos(2\alpha - 4m\beta)) \quad (\text{A.88})$$

$$\text{and} \quad \Delta \dot{u}_{nm} = 2\mathcal{D} \frac{S}{r^2} (a' \cos(2\alpha - 4m\beta)) \quad (\text{A.89})$$

The dissipation rate due to grain boundary diffusion is thus

$$\begin{aligned}\dot{Q}_b &= \frac{1}{V} \frac{1}{2} \frac{1}{\mathcal{D}} \sum_{m=1}^{m=Z} \int_{-r \sin \beta}^{r \sin \beta} j_m^2 dx \\ &= \frac{1}{\pi R_G^2} \sin \beta \mathcal{D} \frac{S^2}{r} \sum_{m=1}^Z \left[ \frac{4}{3} a'^2 \sin^2 \beta \cos^2(2\alpha - 4m\beta) \right] \\ &= \frac{1}{2} \frac{\mathcal{D}}{R_G^3} S^2 \left( \frac{\tan \beta}{\beta} \right)^{\frac{3}{2}} \cos^2 \beta \frac{4}{3} a'^2 \sin^2 \beta\end{aligned}\quad (\text{A.90}).$$

For identifying  $a'$ , one calculates

$$\begin{aligned}\langle \sigma_{22} \rangle &= \frac{1}{V} \sum_{m=1}^{m=Z} \int_{-x}^x x_{2m} T_{2m} dx \\ &= S \cos 2\alpha \left[ 1 - \frac{1}{2} \frac{1}{S} \left( \frac{1}{3} a' \sin^2 \beta + d' \right) \right]\end{aligned}\quad (\text{A.91})$$

The identity  $\langle \sigma_{22} \rangle = S \cos 2\alpha$  thus requires

$$\frac{1}{3} a' \sin^2 \beta + d' = 0 \quad (\text{A.92})$$

It can be verified that the same condition allows meeting the conditions  $\langle \sigma_{11} \rangle = -S \cos 2\alpha$  and  $\langle \sigma_{12} \rangle = S \sin 2\alpha$ .

In order that the diffusion potential be continuous at vertices, the normal traction field,  $T_{nm}$ , must, at vertices, be identical for the two faces:

$$(T_{nm})_{x=r \sin \beta} = (T_{nm+1})_{x=-r \sin \beta} \quad (\text{A.93})$$

which translates into the condition

$$1 - (a' \sin^2 \beta + d') = 0 \quad (\text{A.94})$$

Coupled with Eq. (A.92), this yields

$$a' = \frac{3}{2} \frac{1}{\sin^2 \beta} \quad (\text{A.95})$$

Thus

$$\dot{Q}_{b.} = \frac{3}{2} \frac{\mathcal{D}}{R_G^3} S^2 \left( \frac{\tan \beta}{\beta} \right)^{\frac{3}{2}} \quad (\text{A.96})$$

Finally, for a grain with  $Z = 6$ , the statical bound for  $G_b$  is obtained as

$$\begin{aligned} G_{b_{\text{hexag.}}}^- &= \frac{S^2}{\dot{Q}_{b_{\text{stat}}} + \dot{Q}_{sl_{\text{stat}}}} \\ &= \left( \frac{\pi}{2\sqrt{3}} \right)^{\frac{3}{2}} \left[ \frac{9}{2} + \frac{1}{\eta_b} \frac{1}{4} \frac{\pi}{\sqrt{3}} \right]^{-1} \frac{R_G^3}{\mathcal{D}} \end{aligned} \quad (\text{A.97})$$

## Appendix 1

Eq. (90) is obtained as follows:

$$\begin{aligned}
\Delta \dot{u}_{bn} &= -\frac{dj_b}{d\phi} \frac{d\phi}{ds} = -\frac{1}{R_G} \frac{1}{A(\phi)} \frac{dj_b}{d\phi} \\
j_b &= -2 \frac{\Omega \delta D_b}{kTR_G} S \frac{1}{A^5(\phi)} \left[ \cos 2\alpha \sin 2\phi - \sin 2\alpha \cos 2\phi \left( A^2(\phi) - \frac{e \sin^2 2\phi}{2 \cos 2\phi} \right) \right] \\
j_b &= 2 \frac{\Omega \delta D_b}{kT} \frac{1}{R_G} S \frac{1}{A^5(\phi)} \cos 2\phi \left( A^2(\phi) - \frac{e \sin^2 2\phi}{2 \cos 2\phi} \right) \\
&= 2 \frac{\Omega \delta D_b}{kT} \frac{1}{R_G} S \frac{1}{A^5(\phi)} \left( \frac{a}{b} \cos 2\phi - e \cos^2 \phi \right) \\
\frac{d}{d\phi} \sqrt{\frac{a}{b} - e \cos^2 \phi} &= e \frac{\sin \phi \cos \phi}{\sqrt{\frac{a}{b} - e \cos^2 \phi}} = \frac{e \sin 2\phi}{2 A(\phi)} \\
\frac{d \cos 2\phi}{d\phi A^5(\phi)} &= \frac{1}{A^{10}(\phi)} \left( -2 \sin 2\phi A^5(\phi) - \cos 2\phi \frac{e \sin 2\phi}{2 A(\phi)} \right) = \frac{\sin 2\phi}{A^5(\phi)} \left( -2 - \frac{e \cos 2\phi}{2 A^6(\phi)} \right) \\
\frac{d \cos^2 \phi}{d\phi A^5(\phi)} &= \frac{1}{A^{10}(\phi)} \left( -2 \sin \phi \cos \phi A^5(\phi) - \cos^2 \phi \frac{e \sin 2\phi}{2 A(\phi)} \right) = \frac{\sin 2\phi}{A^5(\phi)} \left( -1 - \frac{e}{2} \frac{1}{A^6(\phi)} \right) \\
\Delta \dot{u}_{bn} &= -\frac{1}{R_G} \frac{1}{A(\phi)} 2 \frac{\Omega \delta D_b}{kT} \frac{1}{R_G} S \frac{\sin 2\phi}{A^5(\phi)} \left[ \frac{a}{b} \left( -2 - \frac{e \cos 2\phi}{2 A^6(\phi)} \right) - e \left( -1 - \frac{e}{2} \frac{1}{A^6(\phi)} \right) \right] \\
&= 4 \frac{\Omega \delta D_b}{kTR_G^2} S \frac{\sin 2\phi}{A^6(\phi)} \left[ \frac{a}{b} + \frac{e}{4} \left( \frac{a \cos 2\phi}{b A^6(\phi)} - 2 - e \frac{1}{A^6(\phi)} \right) \right]
\end{aligned} \tag{A.98}$$